Biomedicine & Pharmacotherapy 203 (2026) 119900

Contents lists available at ScienceDirect

Biomedicine & Pharmacotherapy

journal homepage: www.elsevier.com/locate/biopha

Omega-3 polyunsaturated fatty acids and epigallocatechin-3-gallate attenuate obesity-associated CD44-high stemness in colorectal cancer through modulation of Notch1, Wnt/β-catenin and PI3K/mTOR signaling

Giulia Calafato [a,*], Alice Bernardi [b], Chiara Alquati [b], Dajana Cuicchi [c], Francesco Buttitta [b], Floriana Jessica Di Paola [a], Chiara Pierantoni [d], Claudio Ceccarelli [b], Milena Pariali [b], Giulia Piazzi [e], Luigi Ricciardiello [b,**]

[a] Biobank of Research, IRCCS Azienda Ospedaliero-Universitaria di Bologna, Bologna, Italy
[b] Department of Medical and Surgical Sciences, University of Bologna, Bologna, Italy
[c] IRCCS Azienda Ospedaliero-Universitaria di Bologna, Bologna, Italy
[d] Department of Medical and Surgical Sciences for Digestive, Liver and Endocrine-Metabolic Diseases, IRCCS Azienda Ospedaliero-Universitaria di Bologna, Bologna, Italy
[e] Center for Applied Biomedical Research (CRBA), University of Bologna, Bologna, Italy

ARTICLE INFO

Keywords:
Colorectal cancer
Obesity
Cancer stem cells
Dietary bioactives
Organoids

ABSTRACT

Obesity is a major risk factor for colorectal cancer (CRC), promoting tumor initiation through chronic inflammation and metabolic dysregulation. Cancer stem cells (CSCs) drive CRC progression through Notch1, Wnt/β-catenin (Wnt), and PI3K/mTOR (mTOR) signaling. Omega-3 polyunsaturated fatty acids (EPA and DHA) and epigallocatechin-3-gallate (EGCG) may modulate these pathways. This study investigated the effects of obesogenic-like stimuli on CSC-related CRC signaling and the preventive potential of EPA:DHA-EGCG in patient-derived organoids (PDOs) from normal mucosa (NM) of non-obese (non-OB) patients. CD133 and CD44 expression was evaluated in tumor tissues and matched NM from obese (OB) and non-OB CRC patients. PDOs derived from NM of non-OB patients were exposed to an adipocyte-conditioned medium reproducing an obesogenic adipokine profile, with or without EPA:DHA (1:1) plus EGCG (EDE). Viability, morphology, and molecular markers of stemness, differentiation, and CRC-related pathways were assessed. OB CRC tissues exhibited a CSC change from CD133-high/CD44-low to CD44-high/CD133-low compared with non-OB CRC. In PDOs, OB-EDE recapitulated this CD44-high/CD133-low phenotype, increasing organoid viability and size while maintaining *KRT20* comparable to control (CTRL). *HES1* was significantly upregulated, consistent with modulation of Notch1 signaling. OB-EDE downregulated Wnt target genes and increased the mTOR downstream effector p-S6R. OB + EDE exerted marker- and pathway-specific effects, maintaining *PROM1* at CTRL levels, reducing *CD44* and *HES1*, and increasing *KRT20*, while *LGR5* remained suppressed. Compared with OB-EDE, OB + EDE further reduced the expression of Wnt target genes and reduced p-S6R to CTRL, whereas p-mTOR/mTOR was not significantly affected. Overall, obesogenic-like stimuli were associated with a CD44-high stem-like phenotype accompanied by coordinated changes in Notch1, Wnt and mTOR signaling. EDE exerted differential effects on these molecular alterations, supporting its potential as a complementary bioactive strategy in obesity-associated CRC. Pharmacological inhibition using DAPT provided preliminary functional support for a contribution of Notch1 signaling to the maintenance of this obesogenic phenotype.

1. Background

Colorectal cancer (CRC) is the third most common malignancy worldwide and the second leading cause of cancer-related mortality [1]. Obesity is a critical driver of CRC development and progression acting through chronic inflammation, metabolic dysregulation, and tumor-promoting signaling that influence epithelial transformation into tumor [2,3]. Visceral adipose tissue (VAT) releases adipokines,

* Correspondence to: Biobank or Research, IRCCS Azienda Ospedaliero-Universitaria di Bologna, Via Massarenti 9, Bologna 40138, Italy.
** Correspondence to: Department of Gastroenterology, Hepatology and Nutrition, MD Anderson Cancer Center, 1515 Holcombe Blvd, Houston, TX 77030, USA.
E-mail addresses: giulia.calafato@aosp.bo.it (G. Calafato), lricciardiello@mdanderson.org (L. Ricciardiello).

https://doi.org/10.1016/j.biopha.2026.119900
Received 9 July 2026; Received in revised form 28 August 2026; Accepted 28 August 2026

cytokines, lipids, and metabolites that modulate intestinal epithelial homeostasis. In obese condition, their dysregulation enhances proliferation and stem-like features while impairing differentiation, promoting a permissive microenvironment for tumor initiation and progression [3,4]. From a translational perspective, a major challenge is to elucidate the mechanisms through which obesity-associated factors influence epithelial transformation, identifying valid targets for prevention. Cancer stem cells (CSCs) are key drivers of CRC onset, progression, and therapy resistance, due to their ability of self-renewal and cellular plasticity [5]. Among the most relevant CSC markers, CD133 and CD44 are strongly associated with tumor aggressiveness, chemoresistance, and poor clinical outcomes in CRC [6]. CD133 and CD44 are physiologically expressed in normal adult intestinal stem cells, where they contribute to tissue homeostasis; however, their aberrant expression has been associated with enhanced tumorigenic potential, identifying CSC populations in the intestinal crypt [7–9]. CSCs are tightly regulated by crosstalk among key CRC-driven pathways, including Wnt/β-catenin (Wnt), Notch1, and PI3K/mTOR (mTOR), which collectively control the balance between stemness and differentiation in the intestinal epithelium [10]. Obesity-related stimuli have been shown to perturb CRC-related pathways, suggesting that an obesogenic environment may influence CSC dynamics and signaling crosstalk [3]. However, whether there is a specific coordinated modulation between CSCs and CRC-driven pathways, under an obesogenic-like environment, is not completely understood. Targeting these mechanisms could represent a promising complementary strategy for CRC prevention, particularly in high-risk populations, as obese individuals. Dietary bioactive compounds, as omega-3 polyunsaturated free fatty acids (PUFAs), including eicosapentaenoic free fatty acid (EPA) and docosahexaenoic free fatty acid (DHA), and the polyphenol epigallocatechin-3-gallate (EGCG), have gained increasing attention as modulators of CRC-associated mechanisms. Indeed, they regulate arachidonic acid-derived prostaglandin synthesis, arrest the cell cycle, induce cell apoptosis, suppress angiogenesis, modulate inflammatory response, and attenuate CRC-driven pathways, including Wnt and mTOR [11,12]. This highlights their potential to interfere with early-driver events of CRC development. However, whether a specific bioactive combination can modulate crosstalk between CSCs and CRC-promoting signaling, under obesogenic-like stimuli, remains unclear. Intestinal patient-derived organoids (PDOs) are unique ex vivo models that recapitulate the molecular and histological features of the tissue of origin, enabling controlled investigation of early driver alterations and molecular crosstalk in CRC, including the effects of obesogenic stimuli on epithelial cell fate and the signaling pathways underlying CRC initiation and progression [13,14]. In this study, we aimed to characterize CSC patterns in tumor tissues and matched normal mucosa (NM) of obese (OB) and non-obese (non-OB) CRC patients, and to investigate whether an obesogenic microenvironment may promote early dysregulation of the crosstalk between CSCs and CRC-related pathways in PDOs from NM of non-OB patients. We also investigated whether a bioactive combination of EPA:DHA and EGCG (EDE) could attenuate these obesogenic factor-induced alterations. Overall, this clinical-translational study provides biological insights into the early molecular changes induced by exposure to obesogenic-like microenvironment, including alterations in CSCs and CRC-related signaling, while assessing the potential preventive effects of dietary bioactive compounds in PDO from NM of non-OB patients.

2. Material and methods

2.1. Patient features

The clinical study was approved by the ethical committee of the Sant'Orsola-Malpighi Hospital (EC: EM903–2019 79/2017/Sper/AOUBo, 2019/10/16) (Bologna, Italy), and written informed consent was obtained from all participants in accordance with the Declaration of Helsinki and the Department of Health and Human Services Belmont Report. Twenty-two patients with sporadic colorectal cancer (CRC), aged 51–80 years, with a diagnosis of colorectal adenocarcinoma and eligible for surgical resection (high-risk stage I, stage II, or stage III), were enrolled. Patients were classified as obese (OB) or non-obese (non-OB) based exclusively on waist circumference (WC) (>102 cm in males or >88 cm in females). Body mass index (BMI) was recorded as an additional parameter but was not used for group allocation. Surgically resected specimens, including normal appearing colonic mucosa (NM), colorectal cancer (CRC), and visceral adipose tissue (VAT) were obtained by OB and non-OB patients. To avoid molecular bias, patients with a family history of adenomas or colorectal cancer, hereditary polyposis or non-polyposis syndromes, inflammatory bowel disease, significant weight loss within three months before diagnosis, ineligibility for primary tumor surgery, antibiotic use within the previous month, or planned neoadjuvant therapy were excluded. A minimum distance of 5 cm from the tumor margin was maintained for NM resection.

2.2. Immunohistochemistry and analysis of CD133 and CD44

Tissue samples were formalin-fixed and paraffin-embedded following standard histological protocol. Slides were de-paraffinized and rehydrated in three washes of histological grade xylene followed by ethanol (100%, 95%, and 70%) and deionized water. Antigen retrieval was performed with a citrate buffer (pH 6.0) at 120 °C for 20 min. Immunohistochemistry was performed with Novolink Polymer Detection Systems (Leica Biosystems, #RE7150-CE / RE7150-K) according to the manufacturer's protocol. Slides were incubated overnight at 4 °C with CD133 (Cell Signaling Technology, #64326; dilution 1:1000) and CD44 (Cell Signaling Technology, #37259; dilution 1:1000) antibodies. For immunohistochemistry analysis, ten images per sample were acquired using Leica ICC50 W microscope (Leica Biosystems). The immunohistochemical expression of CD133 and CD44 was evaluated in tissue sections by two independent observers blinded to the clinical data and study group allocation. Patients were stratified into four groups: NM non-OB, CRC non-OB, NM OB, and CRC OB. For each image was assigned an immunoreactivity score (IS, range 0–12), calculated as the product of the extent of staining (0 = no staining; 1 = 1–10%; 2 = 11–25%; 3 = 26–50%; 4 = 51–100%) and staining intensity (0 = none; 1 = weak; 2 = moderate; 3 = strong). For each sample, the mean of IS derived from the two observers was calculated. Median IS values were then determined for each group and normalized to the NM non-OB group to obtain the percentage of membrane positivity for CD133 and CD44, named "Membrane CD133 and CD44 Score". Absolute frequency classes (0–0.9 = Negative; 1–1.4 = Low; 1.5–2.5 = Medium; >2.5 = High) were created according to distribution of CD133 and CD44 membrane positivity. Relative frequency distributions were calculated by dividing the absolute frequency of each class by the total number of samples in the corresponding group and expressing the result as a percentage.

2.3. RNA extraction and RT-qPCR

Total RNA was extracted using ice-cold TRIzol® reagent (Invitrogen™; Thermo Fisher Scientific, #15596026) according to the manufacturer's instructions. RNA concentration and purity were assessed using a NanoDrop 1000 spectrophotometer. Two micrograms of total RNA were reverse-transcribed into cDNA using the High-Capacity cDNA Reverse Transcription Kit with RNase Inhibitor (Applied Biosystems™; Thermo Fisher Scientific, #4374966), following the manufacturer's protocol. Quantitative real-time PCR (RT-qPCR) was performed on a QuantStudio™ 5 Real-Time PCR System (Applied Biosystems™; Thermo Fisher Scientific) using TaqMan™ Fast Advanced Master Mix (Applied Biosystems™; Thermo Fisher Scientific, #4444557) and TaqMan™ Gene Expression Assays (Thermo Fisher Scientific). For NM and CRC tissues, we used *PROM1* (Assay ID:

Hs01009259_m1) and *CD44* (Assay ID: Hs01075864_m1) TaqMan probes. For PDOs, we used the following probes: *AXIN2* (Assay ID: Hs00610344_m1), *MYC* (Assay ID: Hs00153408_m1), *CCND1* (Assay ID: Hs00765553_m1), *LGR5* (Assay ID: Hs00969422_m1), *KRT20* (Assay ID: Hs00300643_m1), *HES1* (Assay ID: Hs00172878_m1), *PROM1* (Assay ID: Hs01009259_m1), *CD44* (Assay ID: Hs01075864_m1) and *RPS6* (Assay ID: Hs03044100_g1). *GAPDH* ((Assay ID: Hs03929097_g1) was used as reference gene for the normalization of qPCR data. Fold change values were calculated using the $2^{-\Delta\Delta Ct}$ method. For CRC tissues, gene expression levels were first normalized to the corresponding NM. Relative fold changes were then expressed as the percentage ratio of CRC non-OB, NM OB, and CRC OB samples over NM non-OB. For PDO experiments, data are expressed as fold change relative to CTRL (mean of treated samples vs CTRL).

2.4. Mature adipocytes isolation and conditioned-medium collection

VAT was collected from four obese patients (PT03, PT09, PT16, PT22) aliquoted and stored at −80 °C. Mature adipocytes were isolated from VAT according to Carswell et al. protocol with some modifications [15]. Briefly, frozen VAT was slowly thawed on ice for at least 2 h. VAT was washed once with PBS and twice with DMEMF12 + 1% penicillin-streptomycin (PS) + 0.1% BSA, then cut into smaller fragments and digested with 220 U/mg collagenase type II (Gibco, #17101–015) in DMEMF12 + 1% PS + 0.1% BSA for 1 h at 37°C. After digestion, the mature adipocytes-containing solution was filtered through a 250 μm filter, diluted 1:1 with DMEMF12 + 1% PS + 0.1% BSA, and centrifuged (400x*g* for 5 min at RT). The supernatant-containing mature adipocytes was transferred into a sterile Petri dish and placed in the incubator. After 5 days, mature adipocytes-derived conditioned-medium, was further diluted 1:1 with DMEMF12 + 1% PS + 0.1% BSA, and therefore called obesogenic conditioned-medium (CM-OB). To validate adipocyte differentiation and assess the quality of the CM-OB collected from mature adipocytes, leptin and adiponectin levels were quantified by ELISA (Supplementary and Figure S1). CM-OB medium was aliquoted and stored at −80 °C until use.

2.5. Patient-derived organoids isolation

NM tissues for organoid isolation were cryopreserved in a DMSO-containing freezing medium at −80 °C until further processing. Four independent patient-derived intestinal organoids (PDO) lines (PT10, PT12, PT13, and PT15) were selected for the planned experiments based on the availability of sufficient cryopreserved NM tissue to complete all experiments. PDO establishment from NM was consistently successful under the culture conditions used, and no PDO cultures were excluded because of failed establishment, contamination, technical issues, or experimental outcome. PDOs were isolated from NM of four non-obese (PT10, PT12, PT13, PT15) patients according to Tsai et al. protocol with some modifications [16]. Briefly, intestinal frozen NM tissue was quickly thawed in water bath at 37 °C and washed once with D-PBS. Tissue fragments were cut into smaller pieces and digested with 220 U/mg collagenase type II (Gibco, #17101–015) in D-PBS for 1 h at 37 °C. The intestinal fragments were centrifuged (600x*g* for 5 min at 4°C) and resuspended with a 1 ml syringe (21 G needle) in DMEMF12 + 1% BSA. After digestion, cells were filtered through a 70 μm strainer, centrifuged and resuspended in PDO medium-Matrigel® (PDO medium:Matrigel ratio = 2:5) (Corning, #356231). A drop of 40 μl/well of cell-matrix mixture was seeded into 48-well plates. After matrix solidification, 400 μL of PDO culture medium supplemented with 2.5 μM of Thiazovivin (Thz) (Sigma-Aldrich, #SML1045) were added. PDOs establishment occurred within 10/15 days. PDO medium was replaced every two days until expansion/seeding procedures. Detailed composition of PDO medium was reported in Table S1. According to Calafato et al., PDO medium did not include R-Spondin1 supplement, as we used PDOs to explore the cross-talk between CRC-related pathways (i.e. PI3K/mTOR) and cancer-stem cells markers [17]. Both the normal mucosa (NM) tissues used for PDO generation and the corresponding CRC specimens were subjected to next-generation sequencing (NGS) to assess the presence of CRC-driving mutations (Supplementary and Table S2). No CRC-associated mutations were detected in the NM tissues used for PDO establishment.

2.6. Organoids culture procedures

For expansion/seeding procedures, PDOs from NM tissues were dissociated to single cells using TrypLE™ Express (Gibco, #12604–013), resuspended 5 times with a 1 ml syringe (21 G needle), and incubated for 30 min at 37°C, vortexing every 5 min. Reaction was stopped with FBS. Organoids were mechanically dissociated with a 1 ml syringe (21 G needle) into a single cell suspension. Cells were centrifuged at 500x*g* for 3 min and counted. For expansion procedures, 15,000 cells/well (40 μl drop/well – PDO medium:Matrigel ratio = 2:5) were seeded in a 48-well plate in PDO medium with 2.5 μM Thz. After 5–7 days, intestinal PDOs were further expanded or collected for seeding, as needed. For viability assay, 2500 cells/well (15 μl drop/well – PDO medium:Matrigel ratio = 2:5) were seeded in 48-well plates in 150 μl of PDO medium supplemented with 2.5 μM of Thz. For RNA/protein biomolecular analysis, 7 drops/well (2500 cells/drop in 15 μl/drop – PDO medium:Matrigel ratio = 2:5) were seeded in 12-well plates in 350 μl of PDO medium with 2.5 μM of Thz. Four independent PDO lines (PT10, PT12, PT13, and PT15), each established from a different patient, were used throughout the study, except for dose-response and DAPT pharmacological inhibition experiments, which were performed using three independent PDO lines (PT12, PT13, and PT15). For each PDO line, one viability assay and one experiment for RNA and protein extraction were performed. Cell viability assays were carried out in technical triplicates for each experimental condition. For molecular analyses, PDOs were seeded in four wells per treatment condition, and material from all four wells was pooled for RNA and protein extraction. For statistical analyses in PDOs, the repeated-measures analyses accounted for the paired structure arising from the evaluation of the same PDO lines across treatment conditions; each independent PDO line was considered one biological replicate, and technical replicates were not treated as independent observations.

2.7. PDO treatments

Four days after seeding, PDOs were treated for 48 h. For dose-response assays, PDOs were exposed to EGCG or EPA:DHA (1:1, w/w). In all other experiments, PDOs were treated with the combined formulation (EDE; EPA:DHA 1:1 plus EGCG) at the indicated concentrations. Vehicle controls consisted of DMSO and 96% ethanol pre-diluted in PBS (1:10 and 1:4, respectively) and added at equivalent final volumes. In dose-response assays, controls and treatments were performed in OB medium (PDO medium:CM-OB, 1:1), whereas in all other experiments, controls consisted of vehicle-containing PDO medium. For OB-related conditions, OB-EDE included vehicle-treated OB medium, while OB + EDE contained EPA:DHA (150 μM, 1:1) and EGCG (60 μM) in OB medium. Media compositions are provided in Tables S1 and S3, and additional details are reported in the Supplementary Information. EGCG was tested at 60–300 μM and EPA:DHA at 15–1000 μM. For optimization, EPA:DHA (150 μM) was combined with EGCG (60–90 μM); the final EDE condition used throughout was EPA:DHA (150 μM) plus EGCG (60 μM).

2.8. PDO viability assay

After treatments (48 h), PDO viability was analyzed by the luminescent-based CellTiter-Glo® 3D Cell Viability Assay (Promega, #G9681), according to the manufacturer's instructions. The

Luminescent signal was measured by the multimode plate reader Spark® (Tecan) (integration time 1000 ms). Reactions were performed in triplicates. Intestinal PDOs viability was expressed as a percentage of the ratio between the mean luminescence of treated samples over CTRL.

2.9. PDO imaging

Intestinal PDOs morphological changes, including total area and darkness, were quantitatively assessed every 8 h for 48 h through the Incucyte® live cell analysis system (Sartorius), and representative imaging and corresponding data analysis was performed using the Incucyte® organoids software module (Sartorius). Total organoid area and darkness were automatically quantified by the dedicated software module from acquired images, providing objective surrogate parameters of organoid growth dynamics and morphological changes as previously described [17].

2.10. PDO harvesting for biomolecular analysis

After 48 h of treatment, PDOs were harvested using Cultrex™ Organoid Harvesting Solution (Bio-Techne, #3700–100–01) according to the manufacturer's instructions. Organoids were washed with cold D-PBS and incubated with harvesting solution for 1 h at 4 °C on an orbital shaker to dissolve Matrigel. Samples were collected in 15 ml tubes and centrifuged at 500 × g for 5 min at 4 °C. Pellets were resuspended in 1 ml cold D-PBS and centrifuged at 7500 rpm for 3 min at 4°C. Then, supernatants were discarded, and pellets were snap-frozen in liquid nitrogen and stored at −80 °C until RNA and protein extraction.

2.11. Protein extraction and Western Blot

Whole-cell lysate (total) proteins were extracted by using RIPA Buffer (Tris-HCL Ph-7.5 25 mM, NaCl 150 mM, Na-Deoxycholate 0.50%, NP-40 1%, SDS 0.10% and water) (Thermo Fisher Scientific). A total of 15 μg of total proteins/sample were separated on 4–12% NuPAGE™ Novex Bis-Tris gels (Invitrogen™, Thermo Fisher Scientific, #NP0335BOX) using the NuPAGE™ MOPS SDS Running Buffer (Invitrogen™, Thermo Fisher Scientific, #NP0001). Then, proteins were transferred onto a nitrocellulose membrane. Membranes were blocked with 5% non-fat milk diluted in PBS with 0.05% Tween® 20 (PBST) and then incubated overnight at + 4 °C with the following primary antibodies: non-phospho (Active) β-Catenin (CST, #8814; dilution 1:2000), Total β-Catenin (CST, #9562; dilution 1:2000), CD133 (CST, #64326; dilution 1:1000), CD44 (CST, #37259; dilution 1:1000), HES1 (Thermo Fischer Scientific, #PA5–28802; dilution 1:1000), phospho-mTOR (CST, #2971; dilution 1:1000), mTOR (CST, #2983; dilution 1:1000), cleaved-Notch1 (CST, #3608; dilution 1:1000) and phospho-S6 ribosomal protein (p-S6R) (Ser235/236) (CST, #2211; dilution 1:2000). GAPDH (1:6000, CST #2118) was used as loading control. After incubation, membranes were incubated with the appropriate secondary antibody (Amersham, #NA934) for 1 h at room temperature. Secondary antibodies were diluted 1:1000 in 2% dried non-fat milk diluted in PBST. Prior to re-probing with different antibodies, the membranes were stripped with RestoreTM Western Blot Stripping Buffer (Thermo Fisher Scientific, #21059), washed in PBST, and blocked in 5% non-fat milk diluted in PBST. Signals were detected with Westar Eta C Ultra 2.0 (Cyanagen, #XLS075) (Bologna, Italy) and Westar Antares (Cyanagen, #XLS0142) chemiluminescent substrates. Images were captured with a ChemidocTM XRS + (Bio-Rad Laboratories) (Hercules, CA, USA). Densitometric analyses were performed with Image-Lab software, version 6.1 (Bio-Rad) to quantify the fold differences in protein expression. Data are expressed as fold change relative to CTRL (mean of treated samples vs CTRL). Uncropped blots for Main Figs. 4 and 5 are shown in Figures S2 and S3, respectively.

2.12. Statistical analysis

Statistical analysis was performed using GraphPad Software 10 (Graph Pad Software Inc., La Jolla, CA, USA). Continuous variables, including age, BMI, and WC were expressed as median and interquartile range (IQR), due to the small sample size and the non-normal distribution of the data. Categorical variables were analyzed using Fisher's exact test (comorbidities: presence vs absence; lymph node involvement: N0 vs N1) between the two groups. For tissue analysis, according to data distribution assessed using the Shapiro-Wilk test, Kruskal-Wallis test followed by Dunn's multiple-comparison test, was applied as appropriate for independent-group analyses. For PDO experiments, repeated-measures one-way ANOVA followed by Tukey's or Dunnett's multiple-comparison test was used for parametric data, whereas the Friedman test followed by Dunn's multiple comparison test was used for non-parametric data, according to the distribution assessed using the Shapiro-Wilk test. For all datasets analyzed using parametric ANOVA, homogeneity of variance was assessed using the Brown-Forsythe test, which did not indicate significant differences in variance among groups. The repeated-measures analyses accounted for the paired structure arising from the evaluation of the same PDO lines across treatment conditions. The experimental unit for PDO experiments was the individual patient-derived organoid line. Technical triplicates were averaged before statistical analysis and were not considered independent biological replicates. No prospective sample size or statistical power calculation was performed, as the study was based on the availability of clinical specimens and PDOs. For PDO experiments, no formal randomization procedure was applied; however, the position of each treatment condition within the organoid culture plates was varied across experiments. Blinding was not feasible during PDO cultures, organoid image acquisition and analysis, RT-qPCR, Western blot, and downstream molecular analyses because treatment allocation was necessarily known during sample processing. Immunohistochemical scoring and tissue image analyses were performed by investigators blinded to the patients' clinical information and study group allocation. Statistical significance was assessed as * $p < .05$, ** $p < .01$, *** $p < .001$, and **** $p < .0001$.

3. Results

3.1. Clinical features of obese and non-obese CRC patients

A total of 22 colorectal cancer (CRC) patients were included in the study and stratified into two cohorts exclusively according to waist circumference (WC): non-obese (non-OB) patients (Table 1, n = 8) have WC ≤ 102 cm in males or ≤ 88 cm in females while obese (OB) patients have WC > 102 cm in males or > 88 cm in females (Table 2, n = 14). Non-OB patients showed a median age of 72.5 years (IQR 67.8–76.3), whereas obese patients had a median age of 67.5 years (IQR 62.3–68.8), indicating a comparable age distribution between cohorts (Mann-Whitney *U* test, p = .161) (Tables 1, 2). Body mass index (BMI) was also significantly higher in OB patients compared to non-OB subjects. The median BMI was 22.5 kg/m^2 (IQR 21.8–24.5) in the non-OB group versus 29.5 kg/m^2 (IQR 26.8–31.6) in the OB group (p = .0006) (Tables 1, 2). As expected, based on the predefined classification criteria, WC was significantly higher in OB patients than in non-OB patients, with median values of 106 cm (IQR 97.8–112.8) and 85 cm (IQR 83.8–100.3), respectively (p = .005) (Tables 1, 2). Dietary status and physical activity levels were comparable between the two groups (Tables 1, 2). According to tumor histopathology, both groups predominantly presented intestinal adenocarcinomas with similar anatomical distribution across the colon and rectum (Tables 1, 2). Regarding tumor staging, all non-OB patients presented with N0 disease, whereas lymph node involvement (N1) was observed only in the OB cohort (2 out of 14 patients). However, this difference did not reach statistical significance (Fisher's exact test, p = .515), likely due to the

Table 1
Clinical features of abdominal non-obese patients.

non-OB ID Patient	Age (yrs)	Dietary status	Physical activity	WC (cm)[a]	Weight (Kg)	Height (m)	BMI	CRC Stage	CRC location	Histopathological diagnosis	Comorbidities	Ongoing therapies
PT04	64	Mixed non vegetarian	Moderate	84	66	1.72	22.31	pT3 N0	Sigmoid colon	Sigmoid adenocarcinoma	Psoriasis	Status post colonoscopy
PT10	80	Mixed non vegetarian	Sedentary	101	72	1.62	27.43	pT1 N0	Ascending colon	Moderately differentiated intestinal-type adenocarcinoma arising in a tubulovillous adenoma, infiltrating the submucosa	NA	NA
PT12	77	Mixed non vegetarian	Moderate	83	65	1.69	22.76	pT2 N0	Rectum	Low-grade intestinal adenocarcinoma infiltrating the submucosa	NA	NA
PT13	51	Mixed non vegetarian	Moderate	77	56	1.65	20.57	Pt2 N0	Sigmoid colon	Invasive intestinal-type adenocarcinoma	NA	NA
PT15	70	Mixed non vegetarian	Sedentary	101	81	1.79	25.28	pT3 N0	Right hemicolon	Low-grade, moderately differentiated intestinal-type adenocarcinoma, invasive	Hypertension; Hypercholesterolemia;	Metoprolol; Semaglutide (Ozempic); Insulin glargine; Acetylsalicylic acid (Cardiasa); Ezetimibe; Ramipril;
PT18	75	Mixed non vegetarian	Moderate	100	66	1.65	24.24	pT4A N0	Ascending colon	Low-grade, moderately differentiated, intestinal-type adenocarcinoma (not otherwise specified), invasive with serosal ulceration	Hypertension; Chronic kidney disease; Hypercholesterolemia; Benign prostatic hyperplasia;	Metoprolol; Amlodipine; Anti-acid (Gaviscon); Rosuvastatin; Ramipril; Acetylsalicylic acid; Pantoprazole; Dutasteride; Alfuzosin;
PT20	76	Mixed non vegetarian	Moderate	84	49	1.64	18.22	pT1 N0	Right hemicolon	Low-grade, moderately differentiated, intestinal-type adenocarcinoma, not otherwise specified	Systemic lupus erythematosus; Microvascular ischemia;	Plaquenil, Delta-cortene, Cardioaspirina
PT23	69	Mixed non vegetarian	Moderate	86	57	1.6	22.27	NA	NA	NA	Hypertension	Zestril

Abbreviations: "/" means none; "NA" means not available.
[a] OB/non-OB classification was based exclusively on waist circumference (WC); BMI was reported as an additional descriptive parameter and was not used for group allocation.

Table 2
Clinical features of abdominal obese patients.

OB ID Patient	Age (yrs)	Dietary status	Physical activity	WC (cm)[a]	Weight (Kg)	Height (m)	BMI	CRC Stage	CRC location	Histopathological diagnosis	Comorbidities	Ongoing therapies
PT03	68	Mixed non vegetarian	Moderate	100	90	1.67	32.27	T1 N1 M0	Descending colon	Adenocarcinoma	Thyroid goiter (hyperthyroidism); Constipation;	Levothyroxine (Eutirox); Vitamin D;
PT05	77	Mixed non vegetarian	Moderate	97	59	1.58	23.63	pT3 N0	Rectum	Adenocarcinoma	Hypertension, Dyslipidemia; Osteopenia; Depressive disorder with anxious features;	Losartan; Diuretics; Atorvastatin; Levosulpiride;
PT06	63	Mixed non vegetarian	Sedentary	106	88	1.78	27.77	pT2 N0	Ascending colon	Adenocarcinoma	Diabetes mellitus; Aortic dissection;	Insulin therapy; antihypertensive medications (aortic dissection);
PT07	52	Mixed non vegetarian	Moderate	109	85	1.79	26.53	pT2 N0	Sigmoid-rectum	Moderately differentiated intestinal-type adenocarcinoma	Seborrheic dermatitis	/
PT08	69	Mixed non vegetarian	Moderate	94	62	1.64	23.05	pT2 N0	Ascending colon	Low-grade, moderately differentiated intestinal adenocarcinoma	Factor V Leiden mutation	/
PT09	62	Mixed non vegetarian	Moderate	125	104	1.77	33.20	pT3 N0	Sigmoid-rectum	Low-grade, moderately differentiated intestinal adenocarcinoma infiltrating the colonic wall.	Hypertension	Losartan
PT11	72	Mixed non vegetarian	Moderate	92	64	1.6	25.00	pT2 N0	Ascending colon	Low-grade, moderately differentiated intestinal-type adenocarcinoma infiltrating the intestinal wall up to the muscularis propria	Hypertension; Diabetes mellitus type 2;	Ramipril; Acetylsalicylic acid; Vitamin D; Saflutan; Allopurinol; Sertraline; Bisoprololo;
PT14	79	Mixed non vegetarian	Moderate	114	89	1.67	31.91	pT1 N0	Ascending colon	Low-grade intestinal adenocarcinoma arising in a tubulovillous adenoma with areas of high- and low-grade dysplasia, infiltrating the submucosa	NA	Losartan; Omeprazole; Acetylsalicylic acid;
PT16	65	Mixed non vegetarian	Moderate	103	80	1.7	27.68	pT4A N0	Transverse-descending colon	Moderately differentiated intestinal-type adenocarcinoma, invasive	Benign prostatic hyperplasia	Alfuzosin (Xatral)
PT17	68	Mixed non vegetarian	Moderate	106	75	1.59	29.67	pT3 N0	Descending colon	Low-grade, moderately differentiated intestinal adenocarcinoma, invasive	Hypertension; Diabetes mellitus type 2;	Trimetazidine (Trulicyl); Clopidogrel (Lobidur); Folic acid (Fulcrosupra); Atorvastatin (Torvast);
PT19	56	Mixed non vegetarian	Moderate	97	91	1.72	30.76	NA	NA	NA	Venous thrombophlebitis	Warfarin (Comadin)
PT21	67	Mixed non vegetarian	Moderate	118	92	1.6	35.94	NA	Right hemicolon	Tubular adenocarcinoma with areas of high- and low-grade dysplasia	Atrial fibrillation (cardioversion)	Apixaban (Eliquis); Hydrochlorothiazide - miloride (Bifrizide); Metoprolol; Omega-3 fatty acids (Omega 3);
PT22	57	Mixed non vegetarian	Moderate	107	98	1.83	29.26	pT4A N1C	Descending colon	Low-grade, moderately differentiated adenocarcinoma, not otherwise specified (NOS), with focal mucinous features, invasive	/	/
PT24	68	Mixed non vegetarian	Moderate	116	87	1.68	30.82	NA	NA	NA	Diabetes mellitus; Hypertension	Metformin; Telmisartan (Blopress);

Abbreviations: "/" means none; "NA" means not available.
[a] OB/non-OB classification was based exclusively on waist circumference (WC); BMI was reported as an additional descriptive parameter and was not used for group allocation.

limited sample size (Tables 1, 2). A higher proportion of metabolic and cardiovascular comorbidities (including diabetes mellitus, hypertension, and dyslipidemia) was observed in OB patients compared to non-OB patients (64% vs 37.5%) (Tables 1, 2). However, this difference was not statistically significant ($p = .40$, Fisher's exact test). Non-OB patients more frequently presented heterogeneous and non-metabolic comorbidities. Despite the lack of significance in some variables, a consistent trend toward a higher metabolic burden and increased anthropometric measures was observed in the obese CRC cohort compared to non-obese patients.

3.2. Differential expression of CD133 and CD44 in obese and non-obese CRC patients

To investigate whether cancer stem cell (CSC) markers are differentially involved in CRC carcinogenesis in the context of obesity, we evaluated the protein levels (immunoreactivity score, IS), and gene expression of CD133 and CD44 (Fig. 1), two of the most relevant CSC markers. CRC patients were stratified based on WC into non-OB and OB groups. For each patient, both normal mucosa (NM) and tumor tissue (indicated as CRC) were collected, resulting in four sample categories: NM non-OB, CRC non-OB, NM OB, and CRC OB. Our results indicate that CD133 protein and gene expression was significantly downregulated in the CRC OB group compared to CRC non-OB (protein: $p < .0001$; gene: $p = .0014$) (Figs. 1A, 1B, 1D). Similarly, NM OB samples exhibited significantly lower expression than NM non-OB (protein: $p < .0001$; gene: $p = .0001$) (Figs. 1A, 1B, 1D). CRC non-OB showed reduced CD133 expression compared to its corresponding NM non-OB (protein: $p = .0004$; gene: $p = .0215$), and CRC OB displayed lower CD133 levels relative to NM OB (protein: $p = .0178$; gene: $p = .0201$) (Figs. 1A, 1B, 1D). As for classes distribution, absolute and relative frequencies (Table 3) highlight that most of CD133-high cases belong to NM non-OB group while most of CD133-negative/low cases belong to CRC OB. A progressive decrease in CD133 IS (Fig. 1B, Table 3) and gene expression (Fig. 1D) was observed across the groups in the following order: NM non-OB, CRC non-OB, NM OB, CRC OB. Conversely, we observed a significant upregulation of CD44 protein (IS) and RNA levels in CRC OB compared to CRC non-OB (protein: $p < .0001$; gene: $p < .0001$) (Figs. 1A, 1C, 1E). Similarly, NM OB samples exhibited higher CD44 expression than NM non-OB (protein: $p = .0014$; gene: $p < .0001$), in a statistically significant way (Figs. 1A, 1C, 1E). CRC non-OB displayed higher CD44 levels than its corresponding NM non-OB (protein: $p < .0001$; gene: $p = .0944$), and the same pattern was observed between CRC OB and NM OB (protein: $p < .0001$: gene: $p = .0088$) (Figs. 1A, 1C, 1E). As for classes distribution, absolute and relative frequencies (Table 4) indicate that most of CD44-high cases belong to CRC OB while most of CD44-negative/low cases belong to NM non-OB. These results highlight that CD44 IS (Fig. 1C, Table 4) and gene expression (Fig. 1E) increases progressively in association with both tumor tissue and obesity status, in contrast to the decreasing pattern observed for CD133.

3.3. Effect of obesogenic-like stimuli and bioactive combination on patient-derived organoids viability

Following the differential expression of CD133 and CD44 observed across the four patient groups, and consistent with previous evidence showing that obesity-associated microenvironments can promote cancer stem cell expansion and activate key oncogenic pathways involved in CRC carcinogenesis [4], we established ex vivo patient-derived intestinal organoids (PDOs) from NM of four non-obese patients and exposed them to obesogenic-like stimuli alone or with a combination of bioactive substances known to modulate CRC-driven pathways. This model allowed us to investigate how obesogenic-like stimuli affect CSC markers expression and its interplay with CRC-related pathways, as well as to assess whether the EDE (EPA:DHA + EGCG) combination could attenuate these alterations. Before evaluating the biological effects of the obesogenic stimulus, we biochemically characterized the adipocyte-conditioned medium (CM-OB). As reported in Supplementary Figure S1, ELISA analysis showed an adipokine profile consistent with an obesogenic microenvironment, characterized by increased leptin levels together with reduced adiponectin levels. This CM-OB was subsequently diluted 1:1 with PDO medium to generate the obesogenic culture medium (OB medium), which was used for both the OB-EDE and OB + EDE experimental conditions throughout all PDO experiments. PDOs were isolated from NM of four non-OB patients. First, we performed dose-response viability curves to evaluate the sub-cytotoxic concentration of either EGCG or EPA:DHA (1:1 ratio), administered as single agents. We found that the sub-cytotoxic concentrations were approximately 60 μM for EGCG (Fig. 2A) and 150 μM for EPA:DHA (Fig. 2B). We subsequently performed 48h-viability assays to optimize the sub-cytotoxic concentration of EDE, a combination consisting of EPA:DHA (1:1) supplemented with EGCG. EPA:DHA concentration was maintained at 150 μM, while EGCG was tested within a range of 60–90 μM. We found that the optimal concentration to maintain a sub-cytotoxic effect in PDOs was 150 μM EPA:DHA supplemented with 60 μM EGCG (Fig. 2F). In contrast, higher EGCG concentrations resulted in a reduction in cell viability (Figs. 2C, 2D, 2E). In our PDO model, the OB-EDE condition, which represents the obesogenic-like stimuli (derived from CM-OB medium from four obese patients) induced a significant increase in PDOs viability (mean difference = −56.89, 95% CI −89.79 to −23.99; $p = .0112$) compared to CTRL. OB + EDE, when used at sub-cytotoxic concentration, attenuate the obesogenic-like (OB-EDE)-dependent increased viability, achieving levels comparable to CTRL (R^2=.8573). Based on these findings, this concentration set was selected for all subsequent PDO culture experiments to evaluate PDO morphology and gene/protein expression of CSC markers and CRC-related pathways.

3.4. Effect of obesogenic environment and bioactive combination on patient-derived organoids morphology

We showed that, in our PDO model, OB-EDE significantly increased PDO viability in 48 h, while OB + EDE was able to attenuate it. We therefore investigated whether obesogenic-like stimuli might alter organoid morphology and whether the EDE combination could modulate these changes. To evaluate this, PDOs derived from NM of four non-OB patients were treated with OB + EDE or OB-EDE for 48 h. Morphological parameters critical for organoid characterization, including organoid total area and darkness, were analyzed, and representative imaging of the assay at 0 and 48 h are shown in Fig. 3A. We observed that organoid total area gradually increased following OB-EDE treatment (Fig. 3B), reaching a maximum at 48 h, which was statistically higher than both CTRL (mean difference = −26.04, 95% CI −31.37 to −20.70; $p = .0006$) and OB + EDE (mean difference = 24.88, 95% CI 15.54 to 34.23; $p = .0032$) conditions (R^2=.9822) (Fig. 3C). In contrast, OB + EDE maintained values comparable to CTRL throughout the time-lapse experiment (Figs. 3B and 3C). No statistically relevant changes in PDO darkness were observed between CTRL and OB + EDE at any time point, while OB-EDE slightly decrease darkness at 48 h (Figs. 3D, 3E). As these parameters provide objective surrogate of organoid growth dynamics and morphological changes, these results are in line with our previous findings of the effect of the obesogenic-like stimuli and bioactive molecule combination on PDO viability.

3.5. Modulation of intestinal cancer-stem cells, differentiation, and Notch1 effector in patient-derived organoids

We next investigated whether obesogenic-like stimuli (OB-EDE) affected the expression of CSC markers and CRC-related pathways involved in stemness maintenance, and whether the EDE combination (OB+EDE) could modulate this effect in our PDO model. We analyzed the expression of key intestinal stemness and differentiation markers -

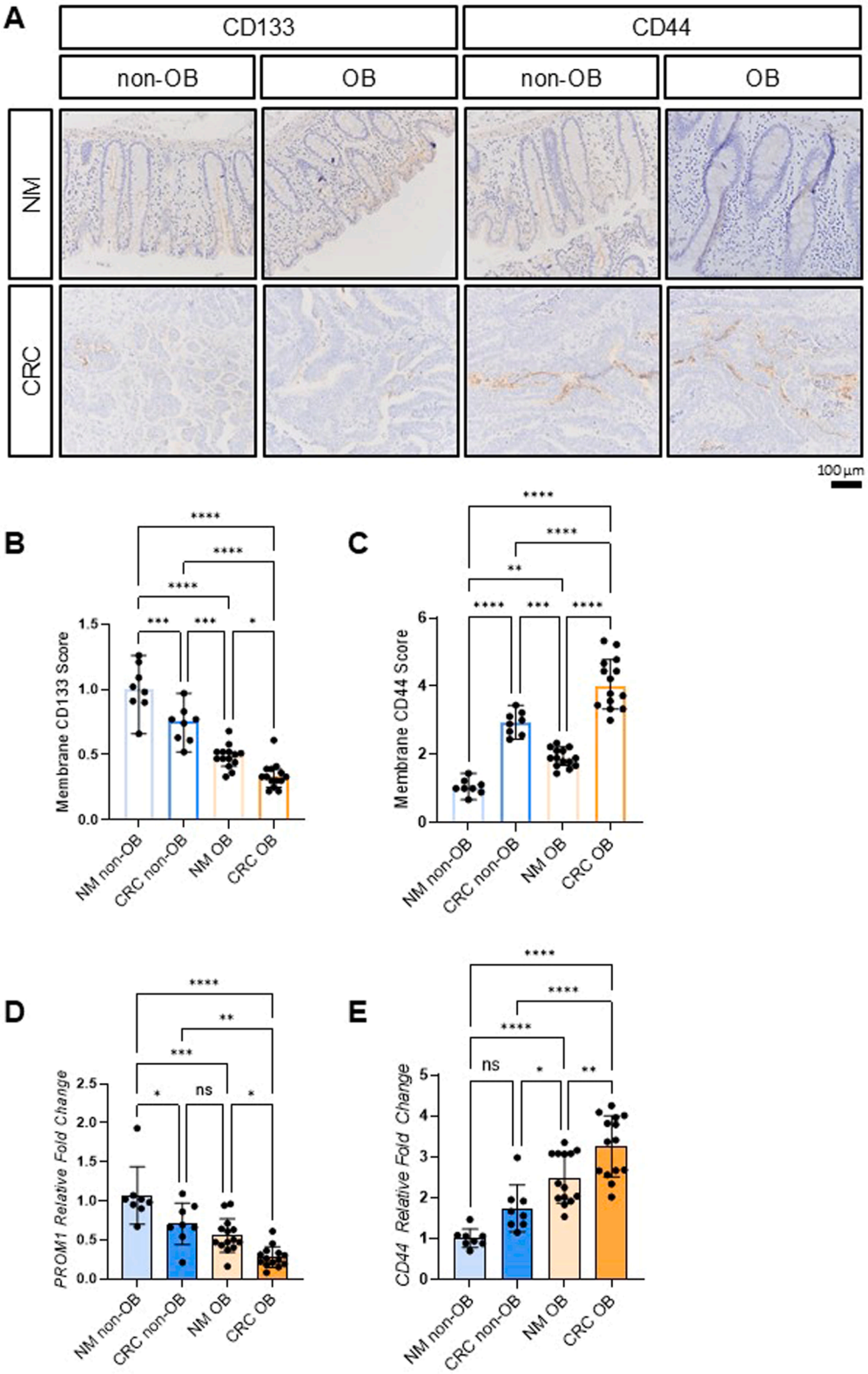

Fig. 1. CD133 and CD44 expression in normal mucosa and colorectal cancer tissues from non-obese and obese patients. A) Representative immunohistochemical images of CD133 and CD44. Images show fields with staining intensities close to the median of the corresponding group. B, C) Quantification of membrane CD133 and CD44 immunohistochemical staining scores. Scale bars: 100 µm; magnification: 200 × . Values were normalized to non-OB NM samples. Data are presented as median (IQR). D, E) *PROM1* and *CD44* gene expression, normalized to the corresponding NM samples and expressed as relative fold change versus non-OB NM. Data are presented as mean ± SD. Kruskal-Wallis with Dunn's multiple comparison was used. (n = 8 non-OB patients; n = 14 OB patients). Global $p < .0001$ for all comparisons.* $p < .05$, ** $p < .01$, *** $p < .001$, **** $p < .0001$.

Table 3
Immunoreactivity score and frequency classes distribution of CD133.

A								
CD133 Score			**Membrane positivity (%)**					
Patient group			**(Median normalized to NM non-OB)**					
NM non-OB (n = 8)			1.0					
CRC non-OB (n = 8)			0.8					
NM OB (n = 14)			0.5					
CRC OB (n = 14)			0.3					
B								
Frequency classes	**Absolute frequency distribution**				**Relative frequency distribution (%)**			
CD133 Membrane	**NM non-OB**	**CRC non-OB**	**NM OB**	**CRC OB**	**NM non-OB (n = 8)**	**CRC non-OB (n = 8)**	**NM OB (n = 14)**	**CRC OB (n = 14)**
0–0.9 Negative	0.0	0.0	0.0	3.0	0.0	0.0	0.0	21.4
1–1.4 Low	0.0	0.0	2.0	9.0	0.0	0.0	14.3	64.3
1.5–2.5 Medium	1.0	3.0	12.0	2.0	12.5	37.5	85.7	14.3
> 2.5 High	7.0	5.0	0.0	0.0	87.5	62.5	0.0	0.0

Table 4
Immunoreactivity score and frequency classes of CD133.

A								
CD44 Score			**Membrane positivity (%)**					
Patient group			**(Median normalized to NM non-OB)**					
NM non-OB (n = 8)			1.0					
CRC non-OB (n = 8)			3.0					
NM OB (n = 14)			1.9					
CRC OB (n = 14)			4.0					
B								
Frequency classes	**Absolute frequency**				**Relative frequency distribution (%)**			
CD44 Membrane	**NM non-OB**	**CRC non-OB**	**NM OB**	**CRC OB**	**NM non-OB (n = 8)**	**CRC non-OB (n = 8)**	**NM OB (n = 14)**	**CRC OB (n = 14)**
0–0.9 Negative	5.0	0.0	0.0	0.0	62.5	0.0	0.0	0.0
1–1.4 Low	3.0	0.0	2.0	0.0	37.5	0.0	14.3	0.0
1.5–2.5 Medium	0.0	3.0	12.0	0.0	0.0	37.5	85.7	0.0
> 2.5 High	0.0	5.0	0.0	12.0	0.0	62.5	0.0	85.7

LGR5, *PROM1*, *CD44* and *KRT20* - in PDOs treated for 48 h with OB + EDE or OB-EDE, using RT-qPCR and Western Blot to assess gene and protein expression (Fig. 4). *LGR5*, *PROM1*, and *CD44* were used as markers of CSCs, while *KRT20* served as an indicator of enterocyte differentiation. We also assessed Notch1 signaling, which is both a key regulator of stem cell maintenance and driver of CRC carcinogenesis. We showed that, while the obesogenic-like environment (OB-EDE) and the bioactive combination (OB+EDE) had a similar effect on *LGR5* gene expression, causing a similar decrease that was significant compared to CTRL ($p = .0044$; $p < .0001$, respectively), they showed distinct effects on *PROM1*, *CD44*, and *KRT20* mRNA levels (Figs. 4A, 4B, 4C, 4D). Indeed, compared to CTRL (mean difference =.4488, 95% CI .2983 to .5992; $p = .0023$) and OB + EDE (mean difference = −.3703, 95% CI −.7098 to −.03073; $p = .0398$), OB-EDE significantly decreased *PROM1* (R^2=.9193) (Fig. 4B), increased *CD44* (mean difference = −.4370, 95% CI −.7040 to −.1700; $p = .0130$; mean difference =.7350, 95% CI .5229 to .7491; $p = .0015$, respectively; R^2=.9657) (Fig. 4C), and reduced *KRT20* (compared to OB+EDE: mean difference = −75.65, 95% CI −104.5 to −10.82; $p = .0270$) to levels comparable with CTRL (R^2=.7595) (Fig. 4D). In contrast, OB + EDE maintained *PROM1* at CTRL levels (Fig. 4B), significantly decreased *CD44* relative to OB-EDE (Fig. 4C), and strongly increased *KRT20* compared with both CTRL and OB-EDE ($p = .0180$; $p = .0270$, respectively) (Fig. 4D). These findings suggest that the obesogenic-like condition (OB-EDE) is associated with a CD44-high stem-like profile with reduced differentiation, whereas EDE selectively modulates these alterations by maintaining *PROM1* at CTRL levels, attenuating *CD44*, and promoting *KRT20* expression. We next evaluated the expression of Notch1 pathway markers, analyzing cleaved-Notch1 and HES1 as upstream and downstream driver of pathway (Figs. 4E, 4F, 4G, 4H). OB-EDE treatment induced a significant upregulation of *HES1* gene expression compared with both CTRL (mean difference = −.5965, 95% CI −1.150 to −.04252; $p = .0412$) and OB + EDE (mean difference =.6383, 95% CI .04159 to 1.235; $p = .0419$) (R^2=.8290) (Fig. 4E). A similar trend was observed at the protein level for HES1 and cleaved-NOTCH1, although these differences did not reach statistical significance (Figs. 4F, 4G, 4H). In contrast, OB + EDE maintained the expression of Notch1 pathway markers similar to CTRL (Figs. 4E, 4F, 4G, 4H). These findings suggest that, in our PDO model, obesogenic-like stimuli (OB-EDE) are associated with a CSC-high/differentiation-low profile, accompanied by modulation of Notch1 signaling, as reflected by the significant increase in *HES1* mRNA and the non-significant trends observed at the protein level. EDE combination (OB+EDE) attenuated the obesogenic-like modulation of CSC-associated markers and induced a more differentiated phenotype, while maintaining Notch1 pathway markers at levels comparable to CTRL.

3.6. Evaluation of Wnt/β-catenin and PI3K/mTOR signaling in patient-derived organoids

We next investigated whether the differential modulation of intestinal stemness, cancer stem cell, and differentiation markers induced by obesogenic-like stimuli and EDE was associated with changes in the interplay between two major CRC-related signaling in our PDO model. Thus, we evaluated key effectors of the Wnt/β-catenin (Wnt) pathway - including *CCND1*, *MYC*, and *AXIN2* gene expression, along with the non-phospho-β-catenin/total β-catenin (non-p-β-catenin/total-β-catenin) protein ratio - and of the PI3K/mTOR (mTOR) pathway, by assessing *RPS6* gene and related phospho-S6R (p-S6R) downstream effector, as well as phospho-mTOR/total mTOR (p-mTOR/mTOR) protein ratio. These analyses were performed in PDOs obtained from NM of non-obese patients treated with either OB + EDE or OB−EDE for 48 h. We observed that, compared to CTRL, OB-EDE treatment led to a significant reduction in all Wnt target genes (*CCND1*: $p = .0070$; *MYC*: $p = .0201$; *AXIN2*: $p = .0057$) and a non-significant decrease in non-p-β-catenin/total-β-catenin protein ratio ($p > .9999$) (Figs. 5A, 5B, 5C, 5D, 5E). Notably, OB + EDE induced a more pronounced significant decrease of *CCND1* ($p = .0471$), *MYC* ($p = .0052$), and *AXIN2* ($p = .0281$) genes

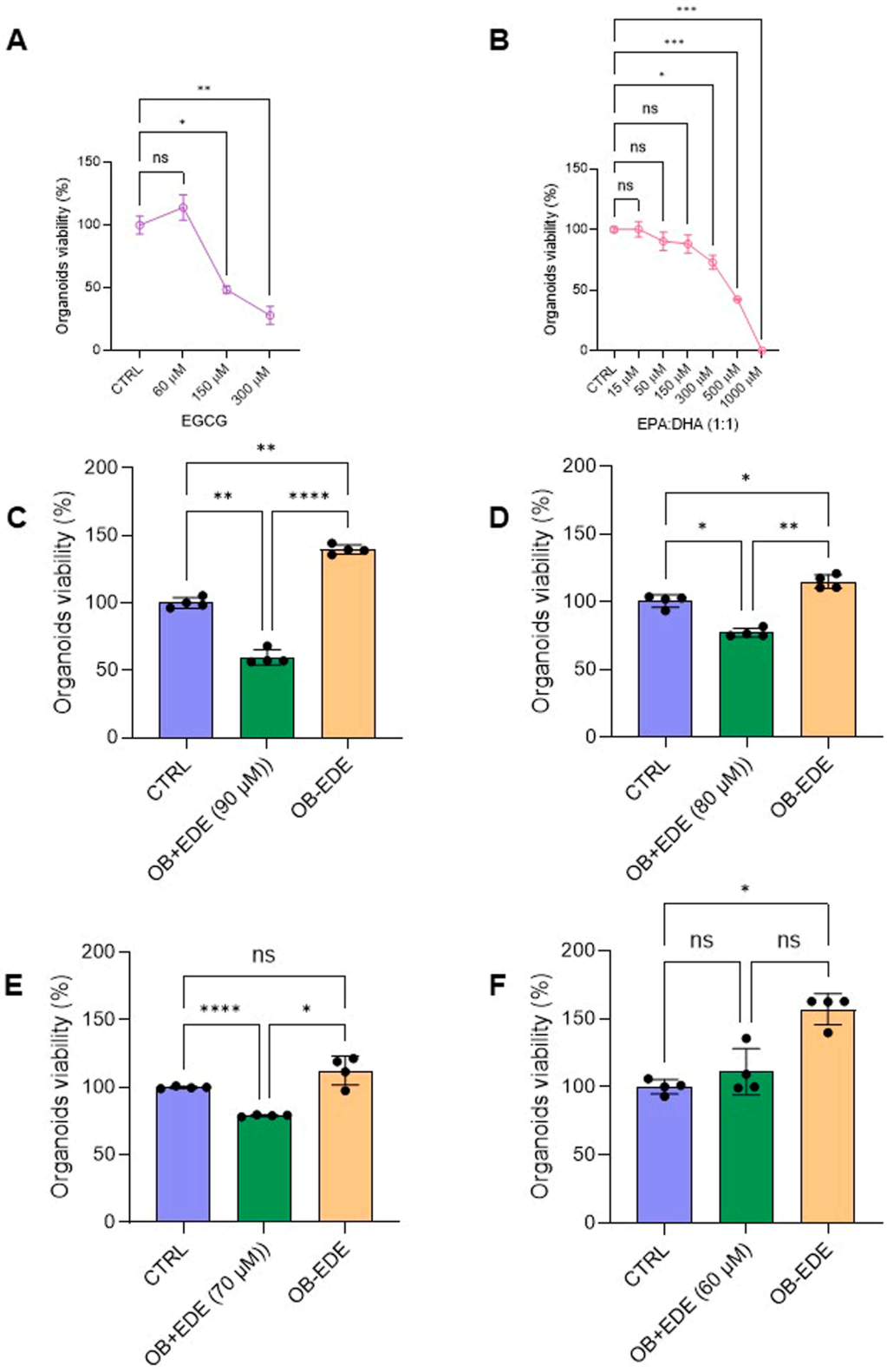

Fig. 2. Effects of obesogenic-like stimuli and bioactive compounds on patient-derived organoid viability. A, B) Dose-response curves for EGCG and EPA:DHA (1:1 ratio) administered as single agents for 48 h in OB medium. CTRL consisted of vehicle-treated PDOs in OB medium. Data are presented as mean ± SD. Repeated-measures one-way ANOVA with Dunnett's multiple comparisons was used (n = 3; PT12, PT13, PT15). C, D, E, F) Optimization of sub-cytotoxic EDE concentrations. EPA:DHA concentration was fixed at 150 µM, while EGCG was tested at 60, 70, 80, 90 µM in OB medium. CTRL consisted of vehicle-treated PDOs in standard PDO medium, whereas OB-EDE consisted of vehicle-treated PDOs in OB medium. Data are presented as mean ± SD. Repeated-measures one-way ANOVA with Tukey's multiple comparisons was used (n = 4; PT10, PT12, PT13, PT15). Global p-values: (A) = .0032; (B) = .0002; (C) < .0001; (D) = .0007; (E) = .0131; F) = .0224. * $p < .05$, ** $p < .01$, *** $p < .001$, **** $p < .0001$.

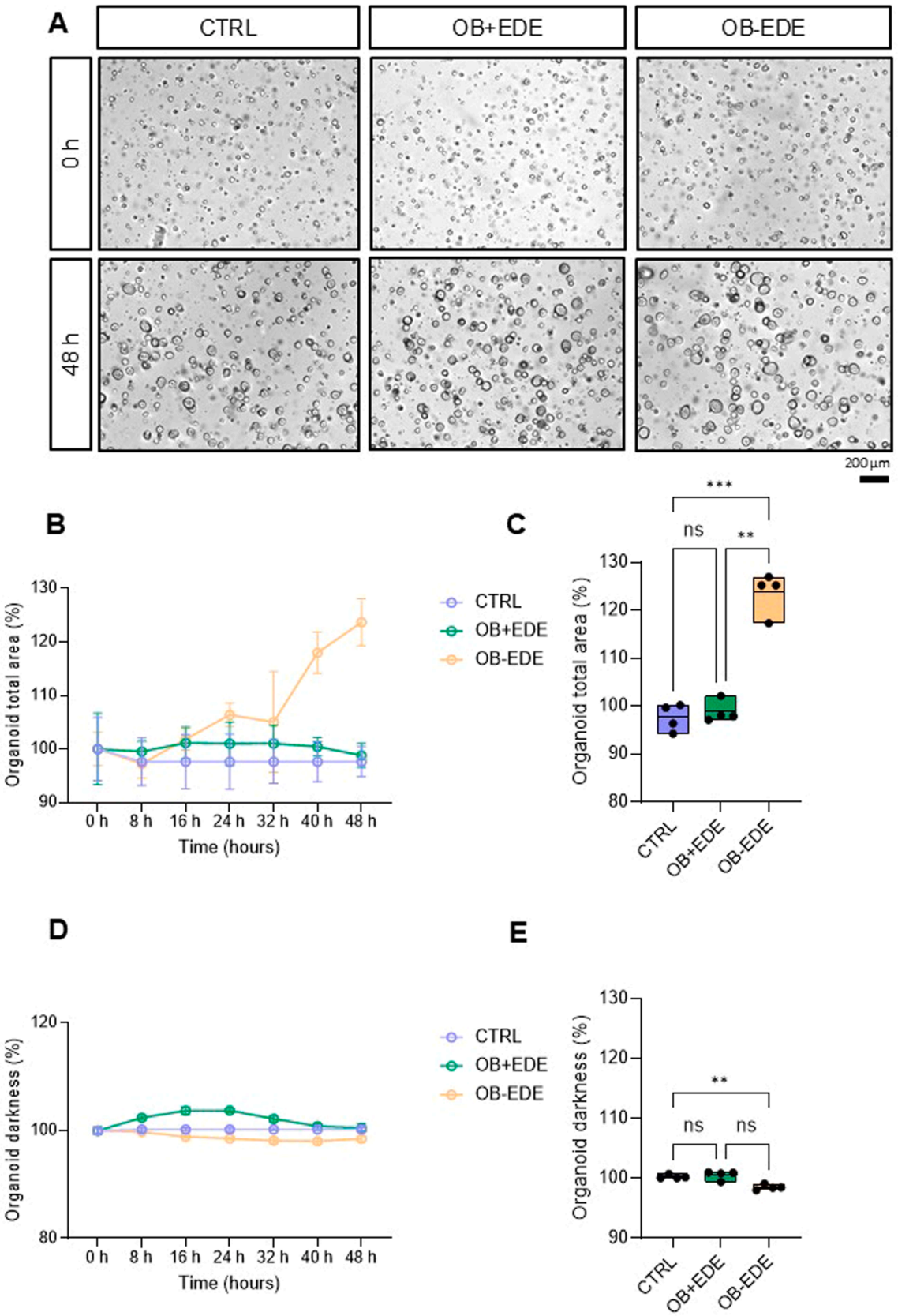

Fig. 3. Effects of obesogenic environment and bioactive combination on patient-derived organoid morphology. A) Representative images of PDOs at 0 and 48 h following treatment with CTRL (vehicle-treated PDOs in standard PDO medium), OB + EDE (150 µM EPA:DHA with 60 µM EGCG in OB medium), or OB-EDE (vehicle pre-diluted in OB medium). B, D) Time-lapse analysis of total organoid area and darkness, respectively, measured every 8 h using the IncuCyte system. C, E) Quantification of total organoid area and darkness, respectively, at 48 h. Repeated-measures one-way ANOVA with Tukey's multiple comparisons was used. Data are presented as mean ± SD (n = 4; PT10, PT12, PT13, PT15). Global p-values: (C) = .0006; (E) = .0418; * $p < .05$, ** $p < .01$, *** $p < .001$, **** $p < .0001$.

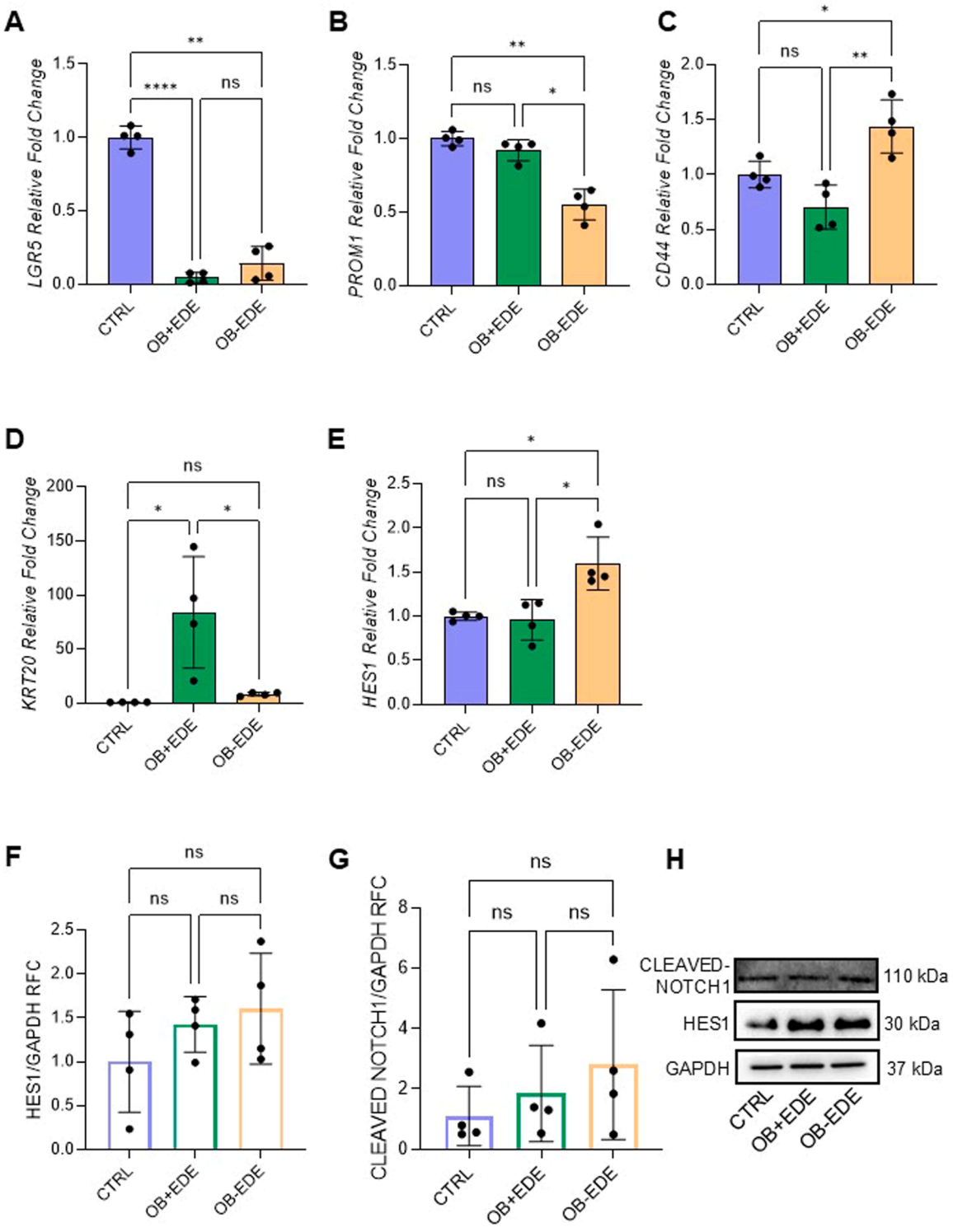

Fig. 4. Transcriptional and protein expression of CSC, differentiation, and Notch1-related markers in patient-derived organoids. A, B, C, D, E) RNA expression of *LGR5, PROM1*, *CD44*, *KRT20*, and *HES1* in PDOs treated for 48 h with CTRL (vehicle-treated PDOs in standard PDO medium), OB + EDE (EDE: 150 μM EPA:DHA with 60 μM EGCG in OB medium) and OB-EDE (vehicle pre-diluted in OB medium). F, G) Western Blot quantification of cleaved-Notch1 and HES1 proteins. H) Representative Western Blot imaging of cleaved-Notch1, HES1 and GAPDH (loading control). Data are presented as mean ± SD (n = 4; PT10, PT12, PT13, PT15). Repeated-measures one-way ANOVA with Tukey's multiple comparisons was used for RNA expression and HES1 protein, whereas Friedman test with Dunn's multiple comparison was used for cleaved-Notch1 protein. Global p-values: (A) = .0012; (B) = .0093; (C) < .0001; (D) = .0139; (E) = .0057; (F) = .3976; (G) = .6528. * $p < .05$, ** $p < .01$, *** $p < .001$, **** $p < .0001$.

and of non-p-β-catenin/total-β-catenin protein ratio, albeit non-significant ($p > .9999$), compared to OB-EDE (Figs. 5A, 5B, 5C, 5D, 5E), indicating that EDE further reduced the transcriptional output of canonical Wnt target genes under obesogenic-like conditions. We next investigated whether the modulation of Wnt signaling under these conditions was coupled to changes in mTOR pathway activity. Analysis of the mTOR pathway revealed that OB-EDE treatment significantly increased the downstream effector p-S6R at both gene (mean difference

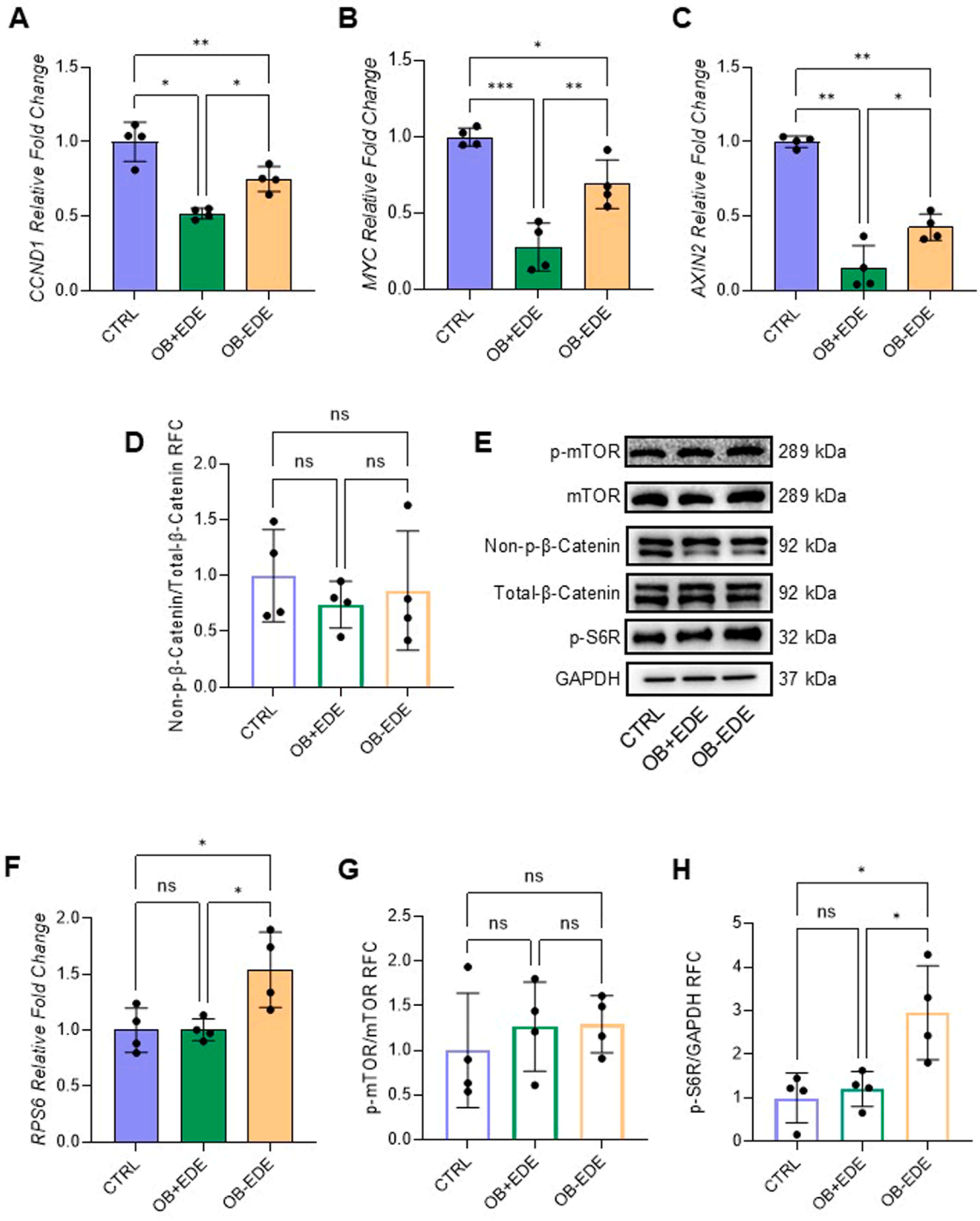

Fig. 5. Transcriptional and protein expression of Wnt/β-catenin and PI3K/mTOR markers in patient-derived organoids. A, B, C) RNA expression of Wnt target genes *CCND1*, *MYC*, and *AXIN2* in PDOs treated for 48 h with CTRL (vehicle-treated PDOs in standard PDO medium), OB + EDE (EDE: 150 μM EPA:DHA with 60 μM EGCG in OB medium) and OB-EDE (vehicle pre-diluted in OB medium). D) Western Blot quantification of non-phospho-β-catenin/total β-catenin. E) Representative Western Blot imaging of phospho-mTOR, total mTOR, non-phospho-β-catenin, total β-catenin, phospho-S6R, and GAPDH (loading control). F) RNA expression of *RPS6*. G, H) Western Blot quantification of phospho-mTOR/total mTOR and phospho-S6R proteins. Data are presented as mean ± SD (n = 4; PT10, PT12, PT13, PT15). Repeated-measures one-way ANOVA with Tukey's multiple comparisons was used for RNA expression, phospho-mTOR/total mTOR and phospho-S6R, whereas Friedman test with Dunn's multiple comparison was used for non-phospho-β-catenin/total β-catenin. Global p-values: (A) = .0075; (B) = .0003; (C) = .0009; (D) = .9306; (F) = .0306; (G) = .5990; (H) = .0227. * $p < .05$, ** $p < .01$, *** $p < .001$, **** $p < .0001$.

= −.5408, 95% CI −1.067 to −.01445; p = .0451; R^2=.6872) and protein (mean difference = −1.958, 95% CI −3.654 to −.2630; p = .0282; R^2=.7167) expression levels compared to CTRL, while only a non-significant increase was observed in p-mTOR/mTOR protein ratio (p = .7824) (Figs. 5E, 5F, 5G, 5H). OB + EDE resulted in p-S6R gene (p = .9999) and protein (p = .9276) levels comparable to CTRL and significantly lower than those observed under OB-EDE (gene: mean difference = .5380, 95% CI .01170 to 1.064; p = .0460; protein mean difference = 1.753, 95% CI .05777 to 3.448; p = .0440) conditions (Figs. 5E, 5F, 5H). In contrast, under OB + EDE treatment, p-mTOR/

mTOR levels remained similar to OB-EDE ($p = .9771$) and slightly higher than CTRL ($p = .8433$), although not reaching statistical significance (Figs. 5E, 5G).

These findings indicate that, in our PDO model, obesogenic-like stimuli were associated with a CD44-high stem-like phenotype characterized by increased *CD44* and *HES1* expression, downregulation of Wnt target genes, and induction of mTOR downstream effector p-S6R, while exerting a more limited effect on upstream mTOR phosphorylation. Conversely, EDE restores epithelial differentiation while attenuating these molecular alterations, notably by reducing Wnt target genes and p-S6R. To further investigate the functional contribution of Notch1 signaling to the obesogenic CD44-high phenotype, three independent PDO derived from NM of non-OB patients (PT12, PT13, and PT15) were treated with the γ-secretase inhibitor DAPT for 48 h under OB-EDE conditions. A preliminary dose-response viability assay identified 5 μM as the optimal sub-cytotoxic concentration, with no detectable effects on PDO viability (Supplementary Figure S4A). Following DAPT treatment (OB-EDE+DAPT), *HES1* expression was significantly reduced compared to OB-EDE (mean difference =.9423, 95% CI .4617 to 1.423; $p = .0049$; R^2=.9243), confirming Notch1 pathway inhibition. This was accompanied by decreased *CD44* (mean difference = 1.121, 95% CI .6159 to 1.627; $p = .0031$; R^2=.9414) and *RPS6* (mean difference = 1.077, 95% CI .6336 to 1.520; $p = .0022$; R^2=.9495) transcript levels across all three PDO models (Supplementary Figure S4B, S4C, S4D).

4. Discussion

In this study, we investigated the impact of obesogenic-like microenvironment on the interplay between cancer stem cells (CSCs) and CRC-driven pathways through an integrated analysis including patient-derived tissues and matched ex vivo patient-derived organoids (PDOs) from normal mucosa (NM) of non-obese (non-OB) patients. We first evaluated the expression of CD133 and CD44, two of the most widely recognized CSC markers, in tumor tissues and corresponding NM of obese (OB) and non-OB CRC patients. Our findings revealed a differential expression pattern associated with both tumor and obesity status, supporting the presence of an obesity-dependent dysregulation of the CSC profile in CRC. Specifically, CD133 expression progressively decreased from NM of non-OB patients to tumor tissues of OB individuals, whereas CD44 displayed the opposite trend. This divergent pattern suggests that obesity may promote a phenotypic change within the CSC compartment, rather than simply affecting CSC abundance. Indeed, although both markers are traditionally linked to stemness, emerging evidence indicates that CD133 and CD44 identify functionally distinct CSC subpopulations with different contributions to tumor progression and cellular plasticity [18,19]. CSC marker dysregulation was already detectable in the NM of non-OB patients (CD133-high/CD44-low) and persisted in tumor tissue of OB patients, where it underwent a phenotypic change toward a CD133-low/CD44-high phenotype, suggesting that obesity is associated with a modification of an early pre-existing CSC imbalance. CD44-high/CD133-low CSC phenotype has been associated with increased tumor aggressiveness and activation of key CRC oncogenic pathways [10,20]. In our obese CRC tissues this phenotypic change is consolidated, suggesting the hypothesis that obesity-associated factors may contribute to CRC development through modulation of CSC phenotype, which may in turn potentiate key CRC-associated molecular pathways. To investigate this hypothesis, we established PDOs from NM of non-OB CRC patients and exposed them to obesogenic-like stimuli (OB-EDE), generating an ex vivo model to investigate the early molecular effects of obesogenic-like stimuli on CSC-associated phenotype and CRC-related pathways. The obesogenic stimuli used in this study were biochemically characterized prior to PDO exposure. ELISA analysis of the adipocyte-conditioned medium (CM-OB) demonstrated increased leptin levels together with reduced adiponectin (Supplementary Figure S1), reproducing the adipokine imbalance typically observed in obese patients. Although our experimental design was not intended to comprehensively characterize the adipocyte secretome or identify the individual soluble mediator responsible for the observed phenotype, this biochemical characterization supports the physiological relevance and reproducibility of our obesogenic stimuli. Among obesity-associated adipokines, the altered leptin/adiponectin profile is consistent with an obesogenic microenvironment and may contribute to the signaling changes observed in PDOs. Previous evidence indicates that obesity-associated changes in leptin and adiponectin contribute to colorectal tumorigenesis while reducing the protective anti-inflammatory and anti-proliferative effects of adiponectin [21]. Under obesogenic-like conditions (OB-EDE), PDOs had higher viability (ATP-viability assay) and size (total area), and lower darkness, consistent with a more metabolically active phenotype. In gene expression analysis, OB-EDE exposure resulted in the upregulation of *CD44* and downregulation of *PROM1*, alongside reduced expression of the differentiation marker *KRT20*, indicating a less differentiated and CD44-driven plastic cellular state. These findings are supported by previous studies showing that a high-fat diet promotes intestinal stemness and tumorigenesis by activating PPARα and PPARδ signaling, thereby inducing a more metabolically active status through fatty acid oxidation (FAO) [4,22]. Furthermore, the detection of a CD44-high/CD133-low CSC phenotype in PDOs, consistent with our findings in patient tissue, supports the validity of our ex vivo models. We observed upregulation of the Notch1 downstream effector *HES1* gene in OB-EDE-treated PDOs. This suggest that CSC plasticity and maintenance of an undifferentiated state may involve CD44- and Notch1-associated signaling rather than a CD133-high phenotype. These findings are in line with Fender et al., who demonstrated that constitutive activation of Notch1 resulted in increased expression CD44 in colon tumor cells, indicating that Notch1 promotes CD44-high stem-like populations and reduces differentiation [23]. While protein-level changes of HES1 did not reach statistical significance, the overall trend is consistent with an impact of obesogenic stimuli on intestinal stemness. To further investigate the functional contribution of Notch1 signaling to the obesogenic CD44-high phenotype, we performed additional pharmacological inhibition experiments using sub-cytotoxic concentration of γ-secretase inhibitor DAPT in three PDOs from NM of non-OB patients. DAPT treatment reduced *HES1* expression, consistent with inhibition of Notch1 signaling, and was associated with decreased *CD44* and *RPS6* levels. Although these analyses were limited to selected molecular markers and were performed only in three independent PDOs, they provide preliminary evidence for a functional contribution of Notch1 signaling to the maintenance of the obesogenic CD44-high phenotype. Exposure of PDOs to obesogenic-like stimuli (OB-EDE) was associated with coordinated changes in CRC-associated signaling. We observed reduced expression of canonical Wnt target genes, including *CCND1*, *MYC*, and *AXIN2*, indicative of attenuation of canonical Wnt transcriptional output, while mTOR downstream signaling was significantly enhanced, as indicated by increased *RPS6* gene and p-S6R protein levels. Although obesity is generally associated with enhanced Wnt/β-catenin (Wnt) signaling during colorectal cancer progression, our experimental model differs substantially from most CRC models because it is based on PDOs established from histologically normal colorectal mucosa rather than established tumors harboring constitutive Wnt pathway activation. The observed reduction in canonical Wnt target gene expression may therefore reflect an early epithelial response to obesogenic stimuli rather than the established Wnt activation typically observed in CRC. This interpretation is consistent with previous studies demonstrating that physiological and oncogenic Wnt responses are distinct in human colon organoids [24]. Whether this finding represents an adaptive feedback mechanism or a transient signaling state preceding later activation of canonical Wnt signaling remains to be determined. Our findings are also consistent with the role of obesity in promoting PI3K/AKT/mTOR pathway in CRC [25,26]. An association between obesogenic stimuli and the mTOR downstream effector p-S6R has not been previously

demonstrated. Therefore, our findings may identify p-S6R as a potential downstream effector associated with the obesogenic response in our PDO model. Our results also align with evidence of negative feedback between Wnt and PI3K-mTOR (mTOR) signaling, in which hyperactivation of mTOR downstream signaling can reduce canonical Wnt transcriptional output [27]. Overall, these findings suggest that obesogenic-like stimuli induce coordinated modulation of CSC, Notch1, Wnt and mTOR pathways, associated with a CD44-high stem-like phenotype. Redox regulation may represent a potential mechanism linking metabolic and microenvironmental cues to CSC plasticity and stemness through redox-sensitive transcription factors, including NRF2 and HIF-1α [28]. Whether redox regulation contributes to the obesogenic-like phenotype observed in our model remains to be determined. In our PDO model, the OB-EDE-associated phenotype may reflect the combined effects of obesity-associated adipokines and other soluble factors within the obesogenic secretome, rather than a single extracellular mediator. The additional DAPT experiments support a preliminary functional contribution of Notch1 signaling to the maintenance of the obesogenic CD44-high phenotype. However, these experiments were designed to assess the preliminary functional contribution of Notch1 inhibition by evaluating representative markers of the Notch1, CSC and mTOR pathways, rather than to comprehensively define the signaling hierarchy. Therefore, the precise hierarchical relationship between Notch1-CD44 or Notch1-mTOR and Notch1, Wnt and mTOR signaling remains to be established. Under obesogenic-like conditions, intestinal plasticity and early tumorigenic features were associated with a CD44-high phenotype and changes in Notch1/mTOR signaling, rather than with the CD133-Wnt profile [29,30]. A recent study showed that a specific cluster of irinotecan-resistant CRC patients exhibited significant enrichment in lipid metabolism and the Notch signaling [31], potentially explaining the association between obesity and Notch1 pathway. The concomitant reduction of Wnt transcriptional output and activation of mTOR downstream signaling suggest that exposure to obesogenic-like stimuli may be associated with changes in signaling networks regulating stemness rather than exclusive reliance on canonical Wnt signaling. Collectively, these findings suggest that obesogenic-like stimuli are associated with a less differentiated, CD44-high stem-like phenotype accompanied by coordinated changes in Notch1, Wnt and mTOR signaling. To investigate the potential preventive effect of a combination of bioactive compounds on the obesogenic-driven tumorigenic effects, we exposed PDOs to EDE (OB+EDE), composed of two polyunsaturated free-fatty acids (PUFAs, EPA:DHA) and the polyphenol (EGCG), under an obesogenic-mimic environment. Importantly, our data indicate that the EDE combination exerted distinct effects on the molecular alterations associated with obesogenic-like stimuli. Compared to OB-EDE, treatment with EDE (OB+EDE) restored PDO viability, total area, and darkness to control levels, indicating that EDE was not cytotoxic and attenuated the effects induced by the obesogenic condition. At the molecular level, compared to OB-EDE, OB + EDE exerted marker-specific effects on CSC-associated and differentiation markers. While *LGR5* remained suppressed relative to CTRL, *PROM1* increased to CTRL levels, whereas *CD44* and *HES1* were reduced toward CTRL levels. In parallel, *KRT20* was significantly upregulated, suggesting a change toward a more differentiated phenotype and attenuation of CD44-high/Notch1-associated state. Interestingly, compared to OB-EDE, OB + EDE condition reduced p-S6R to CTRL at both the gene and protein levels, while further reducing the expression of Wnt target genes, with *AXIN2*, *CCND1* and *MYC* decreasing below CTRL values. These findings are consistent with previous studies demonstrating the anti-tumorigenic effects of omega-3 polyunsaturated fatty acids and EGCG in CRC, where these compounds have been shown to target CSCs and Notch1 and modulate key oncogenic pathways as Wnt/β-catenin and PI3K/mTOR signaling [11,32–35]. However, to the best of our knowledge, this is the first study demonstrating that this specific combination simultaneously modulates Wnt and mTOR signaling while attenuating the obesogenic CD44-high/Notch1 phenotype in PDO from NM of non-OB patients. Our results indicate that EDE differentially modulates the balance between stemness and differentiation markers, maintaining *PROM1* and *HES1* at levels comparable to CTRL, attenuating *CD44*, and increasing *KRT20*. In parallel, EDE further reduced Wnt transcriptional output, while attenuating the obesogenic-dependent increase in the mTOR downstream effector p-S6R. From a translational perspective, these findings provide a biological rationale for further investigating the potential of dietary bioactive compounds in the context of obesity-associated CRC. Obesity is a well-established risk factor for CRC, promoting tumor initiation and progression through chronic inflammation, altered adipokine signaling, and metabolic dysregulation. Our study suggests that early modulation of CSC-associated phenotypes and CRC-signaling networks may represent a potential preventive approach in high-risk settings. In this context, the EPA:DHA-EGCG combination may represent a complementary strategy to modulate early molecular alterations associated with exposure to an obesogenic microenvironment. Given the emerging role of Wnt signaling in shaping the immunosuppressive tumor microenvironment, the modulation of Wnt signaling may also have important clinical implications. Recent evidence indicates that WNT2 blockade can reduce myeloid-derived suppressor cell accumulation and enhance antitumor immunity in CRC [36]. Although our PDO model does not include immune components, these findings support further investigation of whether modulation of obesity-associated phenotype by EDE could influence responses to immune-based therapies. Other studies have already reported the chemopreventive and anti-tumor effects of omega-3 fatty acids and EGCG in different CRC settings (NCT02891538) [37,38]; however, these findings cannot be directly extrapolated to the specific EDE combination investigated here or to obesity-associated CRC prevention. Our findings should not be interpreted as supporting the replacement, reduction, or modification of established oncological treatments for CRC. The potential clinical utility of EPA:DHA and EGCG as complementary preventive strategies remains to be established and requires validation in appropriately designed preclinical and clinical studies. Some limitations should be acknowledged. The relatively small clinical cohort and the limited number of independent PDO models and adipocyte donors may reduce the statistical power and generalizability of our findings and warrants validation in a larger number of independent patient-derived models. Unless otherwise specified, all experiments were performed using four independent PDO lines (PT10, PT12, PT13 and PT15), each established from a different patient, supporting the reproducibility of the observed biological trends. The histological analyses were based on a semiquantitative scoring approach, which, although suitable for assessing the overall expression patterns of CD133 and CD44, may be less sensitive than whole-slides quantitative digital image analysis. PDO experiments were performed using PDO derived from NM of non-OB CRC patients. This experimental design was selected to investigate the early molecular effects of exposure to an obesogenic microenvironment in a non-obese epithelial background and to distinguish changes induced by obesogenic factors from pre-existing obesity-associated alterations. Nevertheless, PDOs derived from NM of obese patients, as well as tumor-derived PDOs from obese and non-obese patients, would have provided additional insight into intrinsic obesity-associated epithelial alterations and further strengthened the translational relevance of the findings. Thus, our model does not fully recapitulate the complex epithelial and tumor-associated features of obesity, and our findings should be interpreted as reflecting obesity-related obesogenic effects rather than the complete spectrum of obesity-driven tumorigenesis. Furthermore, although the adipocyte-conditioned medium was characterized by measuring leptin and adiponectin levels, it represents a complex mixture of adipocyte-derived factors and was not comprehensively characterized. Therefore, the specific contribution of individual adipokines or other soluble mediators cannot be determined, and direct epithelial effects cannot be distinguished from those indirectly mediated by adipocyte-derived factors. Pharmacological inhibition of Notch signaling provided additional mechanistic support for the involvement

of this pathway. However, the lack of complementary genetic or pathway-specific functional studies precludes definitive conclusions regarding the hierarchical relationship between Notch1, Wnt and mTOR signaling. Although active (non-phosphorylated) β-catenin protein was evaluated in whole-cell lysates, nuclear β-catenin was not assessed. Therefore, conclusions regarding canonical Wnt activity should be interpreted with caution and warrant further mechanistic investigation. Last, in vivo validation is lacking, limiting assessment of systemic interactions and long-term effects. Despite these limitations, the integration of patient-derived tissues with PDO-based assays provides a clinically relevant framework to study early obesogenic-driven CRC alterations.

5. Conclusions

In conclusion, our findings in patient-derived tissues and PDO from NM of non-OB CRC patients indicate an association between an obesogenic-like microenvironment and an early CD44-high stem-like phenotype, accompanied by coordinated changes in Notch1, Wnt and mTOR signaling. EDE is associated with marker- and pathway-specific effects, including attenuation of the CD44-high phenotype, promotion of epithelial differentiation, reduction of both mTOR downstream signaling (p-S6R) and Wnt target gene expression, supporting its potential as a complementary preventive strategy in obesity-associated CRC. The Notch-inhibition experiments provide preliminary functional support for a contribution of Notch1 signaling to this obesogenic phenotype, although the mechanistic hierarchy among CSCs and CRC-related pathways remains to be elucidated. Future studies, including functional mechanistic experiments and in vivo validation, will be necessary to confirm these observations and to define the impact of targeting CSC-related pathways in obesity-associated CRC. The clinical utility of EDE remains to be established, and its potential role should be considered complementary to, rather than a replacement for, established oncological treatments.

List of abbreviations

CRC: colorectal cancer
CSCs: cancer stem cells
Wnt: Wnt/β-catenin
mTOR: PI3K/mTOR
PUFAs: omega-3 polyunsaturated fatty acids
EPA: Eicosapentaenoic free fatty acid
DHA: Docosahexaenoic free fatty acid
EGCG: epigallocatechin-3-gallate
NM: normal mucosa
OB: obese
non-OB: non-obese
PDOs: patient-derived organoids
VAT: visceral adipose tissue
EDE: EPA:DHA and EGCG

Authors' contributions

GC conceived and designed the study, performed formal data analysis, coordinated the project, and wrote the original manuscript draft. GC, AB, CA, DC, FB, FJD, CP, CC, MP, and GP contributed to the study methodology. GC, AB, CA and LR performed the investigation. GC and AB curated the data. GC, AB, and CA contributed to data visualization. LR acquired funding and supervised the study. All authors reviewed and edited the manuscript. All authors read and approved the final manuscript.

CRediT authorship contribution statement

Alice Bernardi: Writing – review & editing, Visualization, Methodology, Investigation, Data curation. **Chiara Alquati:** Writing – review & editing, Visualization, Methodology, Investigation, Data curation. **Dajana Cuicchi:** Writing – review & editing, Methodology. **Milena Pariali:** Writing – review & editing, Methodology. **Giulia Piazzi:** Writing – review & editing, Methodology. **Luigi Ricciardiello:** Writing – review & editing, Supervision, Investigation, Funding acquisition. **Giulia Calafato:** Writing – review & editing, Writing – original draft, Visualization, Supervision, Methodology, Investigation, Formal analysis, Data curation, Conceptualization. **Francesco Buttitta:** Writing – review & editing, Methodology. **Floriana Jessica Di Paola:** Writing – review & editing, Methodology. **Chiara Pierantoni:** Writing – review & editing, Methodology. **Claudio Ceccarelli:** Writing – review & editing, Methodology.

Ethics approval and consent to participate

The clinical study was approved by the ethical committee of the Sant'Orsola-Malpighi Hospital (EC: EM903–2019 79/2017/Sper/AOUBo, 2019/10/16) (Bologna, Italy), and written informed consent was obtained from all participants in accordance with the Declaration of Helsinki and the Department of Health and Human Services Belmont Report.

Declaration of Generative AI and AI-assisted technologies in the writing process

During the preparation of this work, the authors used "ChatGPT" solely for linguistic revision and improvement of manuscript readability. After using this tool, the authors reviewed and edited the content as needed and take full responsibility for the content of the published article. All scientific content, data interpretation, and conclusions were developed and verified exclusively by the authors.

Funding

This work was supported by Fondazione Helpida to LR.

Declaration of Competing Interest

The authors declare that they have no known competing financial interests or personal relationships that could have appeared to influence the work reported in this paper.

Acknowledgments

We would like to thank the Department of Medical and Surgical Sciences, University of Bologna, for the support in this research. We thank Center for Applied Biomedical Research (CRBA), University of Bologna, for technical and scientifical support. All authors have read the journal's policy on disclosure of potential conflicts of interest. The authors declare that they have no competing interests.

Appendix A. Supporting information

Supplementary data associated with this article can be found in the online version at doi:10.1016/j.biopha.2026.119900.

Data availability

Data will be made available on request.

References

[1] R.L. Siegel, T.B. Kratzer, N.S. Wagle, H. Sung, A. Jemal, Cancer statistics, 2026, CA Cancer J. Clin. 76 (1) (2026 Jan), https://doi.org/10.3322/CAAC.70043. PubMed PMID: 41528114.

[2] J. Park, T.S. Morley, M. Kim, D.J. Clegg, P.E. Scherer, Obesity and cancer–mechanisms underlying tumour progression and recurrence, Nat. Rev. Endocrinol. 10 (8) (2014) 455–465, https://doi.org/10.1038/NRENDO.2014.94. PubMed PMID: 24935119.

[3] L. Gonzalez-Gutierrez, O. Motiño, D. Barriuso, J. de la Puente-Aldea, L. Alvarez-Frutos, G. Kroemer, R. Palacios-Ramirez, L. Senovilla, Obesity-Associated Colorectal Cancer, Int. J. Mol. Sci. 25 (16) (2024 Aug 1), https://doi.org/10.3390/IJMS25168836. PubMed PMID: 39201522.

[4] S. Beyaz, M.D. Mana, J. Roper, D. Kedrin, A. Saadatpour, S.J. Hong, K.E. Bauer-Rowe, M.E. Xifaras, A. Akkad, E. Arias, L. Pinello, Y. Katz, S. Shinagare, M. Abu-Remaileh, M.M. Mihaylova, D.W. Lamming, R. Dogum, G. Guo, G.W. Bell, M. Selig, G.P. Nielsen, N. Gupta, C.R. Ferrone, V. Deshpande, G.C. Yuan, S.H. Orkin, D. M. Sabatini, Ö.H. Yilmaz, High-fat diet enhances stemness and tumorigenicity of intestinal progenitors, Nature 531 (7592) (2016 Mar 2) 53–58, https://doi.org/10.1038/NATURE17173. PubMed PMID: 26935695.

[5] C.A. O'Brien, A. Pollett, S. Gallinger, J.E. Dick, A human colon cancer cell capable of initiating tumour growth in immunodeficient mice, Nature 445 (7123) (2007 Jan 4) 106–110, https://doi.org/10.1038/NATURE05372. PubMed PMID: 17122772.

[6] X. Lei, Q. He, Z. Li, Q. Zou, P. Xu, H. Yu, Y. Ding, W. Zhu, Cancer stem cells in colorectal cancer and the association with chemotherapy resistance, Med. Oncol. 38 (4) (2021 Apr 1), https://doi.org/10.1007/S12032-021-01488-9. PubMed PMID: 33738588.

[7] J. Zeilstra, S.P.J. Joosten, M. Dokter, E. Verwiel, M. Spaargaren, S.T. Pals, Deletion of the WNT target and cancer stem cell marker CD44 in Apc(Min/+) mice attenuates intestinal tumorigenesis, Cancer Res. 68 (10) (2008 May 15) 3655–3661, https://doi.org/10.1158/0008-5472.CAN-07-2940. PubMed PMID: 18483247.

[8] P. Dalerba, S.J. Dylla, I.K. Park, R. Liu, X. Wang, R.W. Cho, T. Hoey, A. Gurney, E. H. Huang, D.M. Simeone, A.A. Shelton, G. Parmiani, C. Castelli, M.F. Clarke, Phenotypic characterization of human colorectal cancer stem cells, Proc. Natl. Acad. Sci. USA 104 (24) (2007 Jun 12) 10158–10163, https://doi.org/10.1073/PNAS.0703478104. PubMed PMID: 17548814.

[9] L. Zhu, P. Gibson, D.S. Currle, Y. Tong, R.J. Richardson, I.T. Bayazitov, H. Poppleton, S. Zakharenko, D.W. Ellison, R.J. Gilbertson, Prominin 1 marks intestinal stem cells that are susceptible to neoplastic transformation, Nature 457 (7229) (2009 Jan 29) 603–607, https://doi.org/10.1038/NATURE07589. PubMed PMID: 19092805.

[10] N. Ebrahimi, M. Afshinpour, S.S. Fakhr, P.G. Kalkhoran, V. Shadman-Manesh, S. Adelian, S. Beiranvand, F. Rezaei-Tazangi, R. Khorram, M.R. Hamblin, A.R. Aref, Cancer stem cells in colorectal cancer: signaling pathways involved in stemness and therapy resistance, Crit. Rev. Oncol. Hematol. 182 (2023 Feb 1), https://doi.org/10.1016/j.critrevonc.2023.103920. PubMed PMID: 36702423.

[11] A.G. Jayathilake, R.B. Luwor, K. Nurgali, X.Q. Su, Molecular mechanisms associated with the inhibitory role of long chain n-3 PUFA in colorectal cancer, Integr. Cancer Ther. 23 (2024 Jan 1), https://doi.org/10.1177/15347354241243024. PubMed PMID: 38708673.

[12] M. Alam, M. Gulzar, M.S. Akhtar, S. Rashid, Tanuja Zulfareen, A. Shamsi, M. I. Hassan, Epigallocatechin-3-gallate therapeutic potential in human diseases: molecular mechanisms and clinical studies, Mol. Biomed. 5 (1) (2024 Dec 1), https://doi.org/10.1186/S43556-024-00240-9. PubMed PMID: 39725830.

[13] T. Sato, R.G. Vries, H.J. Snippert, M. Van De Wetering, N. Barker, Stange DE, J. H. Van Es, A. Abo, P. Kujala, P.J. Peters, H. Clevers, Single Lgr5 stem cells build crypt-villus structures in vitro without a mesenchymal niche, Nature 459 (7244) (2009 May 14) 262–265, https://doi.org/10.1038/NATURE07935. PubMed PMID: 19329995.

[14] D. Wang, R. Villenave, N. Stokar-Regenscheit, H. Clevers, Human organoids as 3D in vitro platforms for drug discovery: opportunities and challenges, Nat. Rev. Drug. Discov. 25 (3) (2026 Mar 1), https://doi.org/10.1038/S41573-025-01317-Y. PubMed PMID: 41225057.

[15] K.A. Carswell, M.J. Lee, S.K. Fried, Culture of isolated human adipocytes and isolated adipose tissue, Methods Mol. Biol. 806 (2012) 203–214, https://doi.org/10.1007/978-1-61779-367-7_14. PubMed PMID: 22057454.

[16] Y.H. Tsai, M. Czerwinski, A. Wu, M.K. Dame, D. Attili, E. Hill, J.A. Colacino, L. M. Nowacki, N.F. Shroyer, P.D.R. Higgins, J.Y. Kao, J.R. Spence, A method for cryogenic preservation of human biopsy specimens and subsequent organoid culture, CMGH 6 (2) (2018 Jan 1) 218–222.e7, https://doi.org/10.1016/j.jcmgh.2018.04.008. PubMed PMID: 30105282.

[17] G. Calafato, C. Alquati, A. Bernardi, F.J. Di Paola, L. Ricciardiello, Comparative analysis of commercial and home-made media on RSPO1/S6R Axis in organoids with different wnt backgrounds: a methodological guide for the selection of intestinal patient-derived organoids culture media, Int. J. Mol. Sci. 25 (21) (2024 Nov 1), https://doi.org/10.3390/IJMS252111526. PubMed PMID: 39519079.

[18] X. Zhang, L. Yang, W. Lei, Q. Hou, M. Huang, R. Zhou, T. Enver, S. Wu, Single-cell sequencing reveals CD133+CD44−-originating evolution and novel stemness related variants in human colorectal cancer, EBioMedicine 82 (2022 Aug 1), https://doi.org/10.1016/j.ebiom.2022.104125. PubMed PMID: 35785618.

[19] A. Soleimani, N. Saeedi, A.M. Al-Asady, E. Nazari, R. Hanaie, M. Khazaei, E. Ghorbani, H. Akbarzade, M. Ryzhikov, A. Avan, S.M.H. Mehr, Colorectal cancer stem cell biomarkers: biological traits and prognostic insights, Curr. Pharm. Des. 30 (18) (2024 Apr 16) 1386–1397, https://doi.org/10.2174/0113816128291321240329050945. PubMed PMID: 38623972.

[20] J.L. Huang, M. Oshi, I. Endo, K. Takabe, Clinical relevance of stem cell surface markers CD133, CD24, and CD44 in colorectal cancer, Am. J. Cancer Res. 11 (10) (2021) 5141–5154. PubMed PMID: 34765317.

[21] I.E. Vahed, M. Moshgelgosha, A. Kor, M. Minadi, F. Ebrahimi, A. Azhdarian, M. Arjmandi, A. Alamdar, M. Zare, N. Shabani, H. Soltaninejad, M. Rahmanian, The role of Adiponectin and Leptin in Colorectal Cancer and Adenoma: a systematic review and meta-analysis, BMC Cancer 25 (1) (2025 Dec 1), https://doi.org/10.1186/S12885-025-14362-Y. PubMed PMID: 40448255.

[22] M.D. Mana, A.M. Hussey, C.N. Tzouanas, S. Imada, Y. Barrera Millan, D. Bahceci, D.R. Saiz, A.T. Webb, C.A. Lewis, P. Carmeliet, M.M. Mihaylova, A.K. Shalek, Ö. H. Yilmaz, High-fat diet-activated fatty acid oxidation mediates intestinal stemness and tumorigenicity, Cell. Rep. 35 (10) (2021 Jun 8), https://doi.org/10.1016/j.celrep.2021.109212. PubMed PMID: 34107251.

[23] A.W. Fender, J.M. Nutter, T.L. Fitzgerald, F.E. Bertrand, G. Sigounas, Notch-1 promotes stemness and epithelial to mesenchymal transition in colorectal cancer, J. Cell. Biochem. 116 (11) (2015 Nov 1) 2517–2527, https://doi.org/10.1002/JCB.25196. PubMed PMID: 25914224.

[24] B.E. Michels, M.H. Mosa, B.M. Grebbin, D. Yepes, T. Darvishi, J. Hausmann, H. Urlaub, S. Zeuzem, H.M. Kvasnicka, T. Oellerich, H.F. Farin, Human colon organoids reveal distinct physiologic and oncogenic Wnt responses, J. Exp. Med. 216 (3) (2019 Mar 1) 704–720, https://doi.org/10.1084/JEM.20180823. PubMed PMID: 30792186.

[25] C.O. Malley, G.P. Pidgeon, The mTOR pathway in obesity driven gastrointestinal cancers: Potential targets and clinical trials, BBA Clin. 5 (2016 Jun 1) 29–40, https://doi.org/10.1016/j.bbacli.2015.11.003.

[26] D. Wang, J. Chen, H. Chen, Z. Duan, Q. Xu, M. Wei, L. Wang, M. Zhong, Leptin regulates proliferation and apoptosis of colorectal carcinoma through PI3K/Akt/mTOR signalling pathway, J. Biosci. 37 (1) (2012 Mar) 91–101, https://doi.org/10.1007/S12038-011-9172-4. PubMed PMID: 22357207.

[27] A. Prossomariti, G. Piazzi, C. Alquati, L. Ricciardiello, Are Wnt/β-Catenin and PI3K/AKT/mTORC1 Distinct Pathways in Colorectal Cancer? CMGH 10 (3) (2020 Jan 1) 491–506, https://doi.org/10.1016/j.jcmgh.2020.04.007. PubMed PMID: 32334125.

[28] M.Z.J.W.M.L.M. Du, Redox regulation of cancer stem cells: biology and therapeutic implications, MedComm Oncol. 3 (2024) e70005.

[29] D. Horst, L. Kriegl, J. Engel, A. Jung, T. Kirchner, CD133 and nuclear β-catenin: the marker combination to detect high risk cases of low stage colorectal cancer, Eur. J. Cancer 45 (11) (2009) 2034–2040, https://doi.org/10.1016/j.ejca.2009.04.004. PubMed PMID: 19403300.

[30] X. Liang, G.N. Duronio, Y. Yang, P. Bala, P. Hebbar, S. Spisak, P. Sahgal, H. Singh, Y. Zhang, Y. Xie, P. Cejas, H.W. Long, A.J. Bass, N.S. Sethi, An enhancer-driven stem cell–like program mediated by SOX9 blocks intestinal differentiation in colorectal cancer, Gastroenterology 162 (1) (2022 Jan 1) 209–222, https://doi.org/10.1053/j.gastro.2021.09.044. PubMed PMID: 34571027.

[31] Y. Pan, L. Chen, Y. Hu, J. Chang, X. Xu, S.C. Xu, Y.W. Li, J. Du, J.P. Wang, W. Xu, Colorectal cancer organoid model reveals the mechanisms of irinotecan resistance at single-cell resolution, Cancer Med. 15 (2) (2026 Feb 1), https://doi.org/10.1002/CAM4.71550. PubMed PMID: 41678386.

[32] Y. Chen, X.Q. Wang, Q. Zhang, J.Y. Zhu, Y. Li, C.F. Xie, X.T. Li, J.S. Wu, S.S. Geng, C.Y. Zhong, H.Y. Han, -)-Epigallocatechin-3-gallate inhibits colorectal cancer stem cells by suppressing Wnt/β-catenin pathway, Nutrients 9 (6) (2017 Jun 1), https://doi.org/10.3390/NU9060572. PubMed PMID: 28587207.

[33] F. De Carlo, T.R. Witte, W.E. Hardman, P.P. Claudio, Omega-3 eicosapentaenoic acid decreases CD133 colon cancer stem-like cell marker expression while increasing sensitivity to chemotherapy, PLoS. One 8 (7) (2013 Jul 16), https://doi.org/10.1371/JOURNAL.PONE.0069760. PubMed PMID: 23874993.

[34] S. Toden, H.M. Tran, O.A. Tovar-Camargo, Y. Okugawa, A. Goel, Epigallocatechin-3-gallate targets cancer stem-like cells and enhances 5-fluorouracil chemosensitivity in colorectal cancer, Oncotarget 7 (13) (2016 Mar 29) 16158–16171, https://doi.org/10.18632/ONCOTARGET.7567. PubMed PMID: 26930714.

[35] L. D'Angelo, G. Piazzi, A. Pacilli, A. Prossomariti, C. Fazio, L. Montanaro, G. Graziani, V. Fogliano, A. Munarini, F. Bianchi, A. Belluzzi, F. Bazzoli, L. Ricciardiello, A combination of eicosapentaenoic acid-free fatty acid, epigallocatechin-3-gallate and proanthocyanidins has a strong effect on mTOR signaling in colorectal cancer cells, Carcinogenesis 35 (10) (2014 Oct 1) 2314–2320, https://doi.org/10.1093/CARCIN/BGU173. PubMed PMID: 25123131.

[36] C.Z.T.T.L.Q.T.X.H.E.Y.R.J.H.D.L.F. Cui, WNT2 blockade augments antitumor immunity by attenuating myeloid-derived suppressor cells in colorectal cancer, MedComm Oncol. 3 (2024) e70004.

[37] A.J. Cockbain, M. Volpato, A.D. Race, A. Munarini, C. Fazio, A. Belluzzi, P. M. Loadman, G.J. Toogood, M.A. Hull, Anticolorectal cancer activity of the omega-3 polyunsaturated fatty acid eicosapentaenoic acid, Gut 63 (11) (2014 Nov 1) 1760–1768, https://doi.org/10.1136/GUTJNL-2013-306445. PubMed PMID: 24470281.

[38] M.A. Hull, P.L. Ow, S. Ruddock, T. Brend, A.F. Smith, H. Marshall, M. Song, A. T. Chan, W.S. Garrett, O. Yilmaz, D.A. Drew, F. Collinson, A.J. Cockbain, R. Jones, P.M. Loadman, P.S. Hall, C. Moriarty, D.A. Cairns, G.J. Toogood, Randomised, placebo-controlled, phase 3 trial of the effect of the omega-3 polyunsaturated fatty acid eicosapentaenoic acid (EPA) on colorectal cancer recurrence and survival after surgery for resectable liver metastases: EPA for Metastasis Trial 2 (EMT2, BMJ Open. 13 (11) (2023 Nov 29), https://doi.org/10.1136/BMJOPEN-2023-077427. PubMed PMID: 38030258.